

## The doping process and dopant characteristics of GaN

This article has been downloaded from IOPscience. Please scroll down to see the full text article.

2002 J. Phys.: Condens. Matter 14 R657

(<http://iopscience.iop.org/0953-8984/14/22/201>)

View [the table of contents for this issue](#), or go to the [journal homepage](#) for more

Download details:

IP Address: 171.66.16.104

The article was downloaded on 18/05/2010 at 06:45

Please note that [terms and conditions apply](#).

## TOPICAL REVIEW

# The doping process and dopant characteristics of GaN

**J K Sheu and G C Chi**

Optical Sciences Centre, National Central University Chung-Li 32054, Taiwan

Received 6 December 2001, in final form 16 April 2002

Published 23 May 2002

Online at [stacks.iop.org/JPhysCM/14/R657](http://stacks.iop.org/JPhysCM/14/R657)**Abstract**

The characteristic effects of doping with impurities such as Si, Ge, Se, O, Mg, Be, and Zn on the electrical and optical properties of GaN-based materials are reviewed. In addition, the roles of unintentionally introduced impurities, such as C, H, and O, and grown-in defects, such as vacancy and antisite point defects, are also discussed. The doping process during epitaxial growth of GaN, AlGa<sub>1-x</sub>GaN, InGa<sub>1-x</sub>GaN, and their superlattice structures is described. Doping using the diffusion process and ion implantation techniques is also discussed. A p–n junction formed by Si implantation into p-type GaN is successfully fabricated. The results on crystal structure, electrical resistivity, carrier mobility, and optical spectra obtained by means of x-rays, low-temperature Hall measurements, and photoluminescence are also discussed.

**1. Introduction**

The III–V nitride semiconductors have great potential for use in optoelectronics and high-temperature electronic devices due to their wide band gaps and high-temperature stability. Controlling the p-type doping level in wide-band-gap semiconductors is always a challenging task. The doping process can be affected by grown-in defects and unintentional introduction of impurities which may cause self-compensation. In GaN-based materials, some specific grown-in defects were suggested to play an important role, which results in a low doping efficiency of p-type GaN. Many important breakthroughs for group III nitride semiconductors and related devices have been reviewed by Pearton *et al* [1]. The first growth of low-resistivity Mg-doped p-type GaN by metal–organic vapour phase epitaxy (MOVPE) with low-energy electron-beam irradiation (LEEBI) treatment was achieved by Amano *et al* [2] in 1989. In a later work, growth of high-quality Mg-doped p-type GaN treated by thermal annealing in N<sub>2</sub> ambient was also achieved by Nakamura *et al* in 1991 [3]. Despite the achievement of high-quality p-type GaN, the activation efficiency of p-type dopants was still as low as a few per cent. Recent investigations have indicated that using Mg-doped AlGa<sub>1-x</sub>GaN/GaN strained layer superlattices can increase the ionization percentage of acceptors [4–6]. In contrast to p-doped GaN, n-type GaN is easy to produce with high activation efficiency and doping controllability, especially for Si doping [7–12]. For silicon integrated-circuit technologies, ion implantation is one of the most

commonly used processes. It is particularly useful for achieving shallow junctions and isolation profiles across semiconductor wafers. For GaN, Pankove and co-workers [13, 14] were the first to study ion implantation, in 1974. They reported primarily on the photoluminescence (PL) properties of GaN implanted with a long list of elements. No electrical properties were reported, because highly resistive GaN films result from the implantation process. In the early 1990s, studies of ion implantation for GaN were mostly aimed at the realization of p-type materials. Only a few successes in producing p-type GaN were achieved by the ion implantation technique [15, 16]. It is well known that the activation efficiency of implanted impurities and the removal of implantation-induced damage in semiconductors were the critical issues. Unfortunately, the ionization energies of p-type dopants, such as Zn, Mg, Be, and Cd, implanted in GaN are significantly large [17]. In addition, theoretical estimation set the melting temperature of GaN at around 2500 °C (at 4.5 GPa) [18]. Thus, the best annealing temperature could be as high as ~1600 °C. However, care should be taken in the annealing process to maintain the crystal stoichiometry, since GaN will dissociate and sublime at temperatures well below 1600 °C.

In this article, our current understanding of incorporation of native defects and impurities will be addressed, and then we focus on the doping characteristics for intentional introduction of donor and acceptor impurities.

## 2. Role of defects and impurities in group III nitride semiconductors

The high n-type background carrier concentration of undoped GaN has been attributed to nitrogen vacancies and Si and/or O impurities. At a typical epitaxial growth temperature (900–1050 °C), the vapour pressure over the GaN exceeds 760 Torr and irreversible decomposition leading to the formation of nitrogen vacancies occurs [19]. Maruska and Tietjen [20] argued that the n-type background is due to native defects, probably nitrogen vacancies, because the concentration of impurities was two orders of magnitude lower than the electron concentration in their samples. Despite the larger uncertainty in the experimental determination of the impurity concentration, the statement that unintentional n-type GaN doping is due to nitrogen vacancies had been accepted in GaN-related literature. As regards the origins of autodoping, theoretical calculations give conflicting views. The calculations of Perlin *et al* suggested that two native defects, the nitrogen vacancy and interstitial gallium, are responsible for the n-type backgrounds [21]. However, the nitrogen vacancies are likely to be more abundant than the interstitial Ga, because of its lower formation energy. In one study, Zhang *et al* [22] proposed that nitrogen vacancies constitute one of the major sources of autodoping when the carrier concentration  $n < 2 \times 10^{17} \text{ cm}^{-3}$ , but the main sources should be other defects when  $n > 2 \times 10^{17} \text{ cm}^{-3}$ . On the other hand, Neugebauer and Van de Walle [23] reported that achieving thermodynamically stable formation of nitrogen vacancies in n-type GaN in substantial quantities is extremely difficult. They proposed that  $\text{O}_\text{N}^+$  and  $\text{Si}_\text{Ga}^+$  have lower formation energies than  $\text{V}_\text{N}$ , and form shallow donors in GaN. They also suggested that the formation of Ga vacancies could be assisted by complex formation with donor impurities. It is well known that these impurities can be readily incorporated in n-type GaN. In addition, some reports confirmed that unintentionally doped n-type GaN samples contain Si and/or O concentrations consistent with the observed electron concentrations [24–29]. In view of the driving force for the complex formation, an impurity is most likely to form a stable complex with a  $\text{V}_\text{Ga}$  (gallium vacancy) and a donor, since a negatively charged  $\text{V}_\text{Ga}$  acceptor and a positively charged donor attract each other and gain energy by forming a complex. In the light of these findings, Neugebauer and Van de Walle suggested that Si and O form the complexes  $\text{V}_\text{Ga}-\text{Si}_\text{Ga}^+$  and  $\text{V}_\text{Ga}-\text{O}_\text{N}^+$ , which are responsible for the yellow luminescence of n-type GaN. In another

theoretical study, Boguslawski *et al* [30] adopted an *ab initio* molecular dynamics approach to evaluate the effect of cation and anion vacancies, antisites, and interstitials. Although the numerical analyses are comparable, their interpretation differs from the results of Neugebauer and Van de Walle [23]. They suggested that the nitrogen vacancies are responsible for the n-type background of undoped GaN. The formation energies of neutral N and Ga vacancies based on the calculations of Boguslawski *et al* [30] are 3.2 and 8.1 eV, respectively. Under Ga-rich conditions, these vacancies lead to a higher probability of forming  $V_N$  and  $V_{Ga}^{3-}$  although the formation energies of the defects in the highly charged state may be reduced by up to 10 eV. For n-type materials, the energy gain associated with transferring three electrons from the Fermi level to the lower acceptor states of the vacancy makes  $V_{Ga}^{3-}$  the common native defect. In p-type materials, this phenomenon takes place for  $Ga_i^{3+}$  (Ga interstitials) where three donor electrons are transferred to acceptor levels. Therefore, p-type doping of GaN under thermal equilibrium leads to very strong self-compensation effects. Recently, Kim *et al* [31] attempted to establish the origin of the n-type conductivity of unintentionally doped GaN using films and different ammonia flow rates while keeping all other experimental conditions unchanged. The impurity levels and free-carrier concentrations were determined by secondary-ion mass spectrometry (SIMS) and Hall-effect measurements, respectively. Autodoping levels varying with the ammonia flow rates were clearly displayed. It was assumed that the  $V_N$  (nitrogen vacancy) concentration is in inverse proportion to the ammonia flow rate during growth, in the light of author's statements; this finding could support the nitrogen vacancy argument, but it would not rule out the  $O_N$  (substitutional O on N site) argument. To further verify whether the autodoping resulted from native defects or Si and/or O, the depth profiles of impurities were determined by SIMS measurements. Kim *et al* [31] compared the SIMS depth profiles of Si and O with the background for the samples grown with different ammonia flow rates. The background carrier concentrations of the samples ranged from  $3 \times 10^{16}$  to  $2 \times 10^{18} \text{ cm}^{-3}$ . They concluded that the Si impurity levels are lower than  $10^{17} \text{ cm}^{-3}$  for these samples, regardless of the different background electron concentrations. Therefore, it seems reasonable to suggest that the Si impurity is not a major origin of the autodoping of their unintentionally doped GaN films. The source of oxygen was often the  $NH_3$  precursor used in the MOCVD growth, the residual moisture in the MBE chamber, or oxygen impurities leached from a quartz containment vessel (these are commonly used with a  $N_2$  plasma source). The residual moisture in the ammonia is decreased by purification, which therefore reduces the amount of O in GaN. According to the SIMS data of Kim *et al*, the background carrier concentrations seem unaffected by the O concentrations. Thus, autodoping of GaN films caused by nitrogen vacancies is a more logical explanation. In addition, both the H and O contents are proportional to the ammonia flow rates. Therefore, the assumption that both residual O and residual H come from the ammonia is reasonable. Although the influence of O and H in unintentionally doped n-type GaN is minor, their role may be crucial in p-type GaN.

Despite the origin of autodoping in GaN remaining controversial, it is well known that the resistivity of unintentionally doped GaN depends strongly on the growth parameter of the low-temperature nucleation layer. For example, the threading dislocation density and the autodoping level in GaN are strongly related to the thickness of the low-temperature nucleation layer. This indirectly shows that the autodoping level is related to structural defects rather than residual impurities. For  $Al_xGa_{1-x}N$ , the band gap increases with increasing Al content like with the application of hydrostatic pressure [32]. The behaviour of impurities in  $Al_xGa_{1-x}N$  should therefore be similar to that in GaN under pressure. First-principles calculations for O in GaN under pressure show a DX-like transition in which a deep centre incorporating a donor atom together with another constituent forms a complex. One typical DX centre is Si in GaAs, which undergoes a transition from a shallow to a deep centre when hydrostatic pressure

is applied. Under high-pressure conditions the O may move off the initially substitutional donor site [33]. Van de Walle suggested that the DX transition for oxygen in  $\text{Al}_x\text{Ga}_{1-x}\text{N}$  when  $x > 0.3$  is consistent with the observed decrease in n-type conductivity of unintentionally doped  $\text{Al}_x\text{Ga}_{1-x}\text{N}$  [34–37]. In 1982, Yoshida *et al* [34] demonstrated that for  $\text{Al}_x\text{Ga}_{1-x}\text{N}$  grown by MBE, the background carrier concentration varied from  $1 \times 10^{20}$  to  $1 \times 10^{17} \text{ cm}^{-3}$  as the Al content changed from  $x = 0$  to 0.4. In addition, the Hall mobilities were low and did not change with the Al content. In a latter study, Khan *et al* [35] also reported that  $\text{Al}_x\text{Ga}_{1-x}\text{N}$  films grown by MOVPE have a similar characteristic background carrier concentration as a function of Al content. However, in contrast with the findings of Yoshida *et al*, those of Khan *et al* indicated that the Hall mobility decreased with increasing Al composition. A rapid increase in the resistivity of  $\text{Al}_x\text{Ga}_{1-x}\text{N}$  films with increasing Al content was also observed. This phenomenon could be attributed to the formation of oxygen DX centres, which act as negatively charged acceptors compensating the n-type conductivity. On the other hand, Shin *et al* [38] showed that  $\text{Al}_x\text{Ga}_{1-x}\text{N}$  films grown at lower temperature ( $1000^\circ\text{C}$ ) exhibited higher carrier concentrations ( $n > 10^{17} \text{ cm}^{-3}$ ) and lower mobilities ( $\mu \leq 5 \text{ cm}^2 \text{ V}^{-1} \text{ s}^{-1}$ ). When the films were grown at  $1050^\circ\text{C}$ , they exhibited background carrier concentrations and mobilities of  $< 10^{17} \text{ cm}^{-3}$  and  $100\text{--}200 \text{ cm}^2 \text{ V}^{-1} \text{ s}^{-1}$ , respectively. Shin *et al* proposed a model involving native donors to explain their results. However, the data from SIMS measurements revealed oxygen concentrations over  $10^{19} \text{ cm}^{-3}$  and hydrogen, carbon, and silicon concentrations over  $10^{18} \text{ cm}^{-3}$ . As the films were treated with hydrogen plasma, the carrier concentrations were lower than for the as-grown samples. Polyakov *et al* [39] suggested that this behaviour was the result of the passivation of native defects. Also, complexes formed by passivation increased in stability with increasing Al content. The details will be discussed in the following sections.

### 3. Doping during growth

High-quality group III nitride semiconductors with well-controlled doping, composition, and thickness can be grown by MBE and MOVPE. This section covers the doping of group III nitride semiconductors during MOVPE growth. The first breakthrough for group III nitride semiconductors was the use of an AlN [40] or GaN [41] low-temperature nucleation layer for the growth of GaN-based materials. It is possible to obtain high-quality GaN with a specular surface, a low residual carrier concentration, and a high carrier mobility, if the nucleation layers are used to overcome the large lattice mismatch between GaN and sapphire or SiC [40–45]. The second breakthrough was the success in obtaining low-resistivity p-type GaN by using LEEBI [2] or  $\text{N}_2$ -ambient thermal post-annealing for Mg-doped GaN [3, 46]. With the use of these striking techniques, GaN p–n junction light-emitting diodes (LEDs) were fabricated for the first time in 1991 [46]. In most cases, unintentionally doped group III nitride materials are n-type as grown by MOVPE. Under the appropriate growth conditions, this residual doping level can be reduced to levels low enough to allow controllable doping to obtain both n-type and p-type GaN. In this section, the current status and the past development of doping in MOVPE-grown group III nitride materials will be discussed.

#### 3.1. n-type materials

**3.1.1. GaN.** As is generally known, silicon is the most used dopant for classical n-type III–V semiconductors. It can act as a donor or acceptor depending on at which site it is substituted (for a group III or group V element). Under specific growth conditions, it can be incorporated as an acceptor; for example, in liquid-phase epitaxial growth [47]. In GaN, Si mainly substitutes

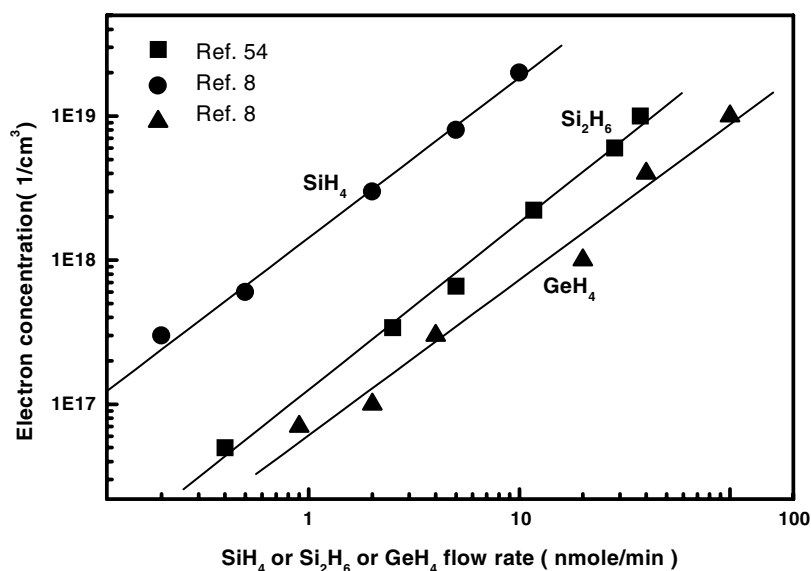


Figure 1. Carrier concentrations of Si- and Ge-doped GaN films as functions of the flow rates of SiH<sub>4</sub>, Si<sub>2</sub>H<sub>6</sub>, and GeH<sub>4</sub>.

at the gallium site due to the low covalent radii difference between Si and Ga, compared with the radii difference from nitrogen. The most popular Si doping sources are SiH<sub>4</sub> and Si<sub>2</sub>H<sub>6</sub> in MOVPE growth. Controllable doping of n-type GaN grown by MOVPE using SiH<sub>4</sub> has been demonstrated over a wide range of concentrations [7–9]. Murakami *et al* [9] showed that the carrier concentration of Si-doped GaN could be as high as  $5 \times 10^{18} \text{ cm}^{-3}$ , but cracks and pits were observed on the highly Si-doped GaN surfaces. However, Nakamura *et al* [8] reported that the carrier concentration could reach  $2 \times 10^{19} \text{ cm}^{-3}$ , with no cracks or pits observed on the surfaces.

Disilane (Si<sub>2</sub>H<sub>6</sub>) is much more reactive than SiH<sub>4</sub> and has been used as a source for Si doping of GaAs. The doping behaviour in Si incorporation into GaAs was found to be temperature independent in the range of 600–800 °C [48]. Similar results were reported for Si-doped InGaP [49]. Thus, the use of Si<sub>2</sub>H<sub>6</sub> rather than SiH<sub>4</sub> may result in better repeatability and uniformity in n-type doping profiles for GaAs. Therefore, it is of interest to investigate Si doping of GaN by using Si<sub>2</sub>H<sub>6</sub>. The carrier concentration of Si-doped GaN as functions of the flow rates of Si<sub>2</sub>H<sub>6</sub> and SiH<sub>4</sub> are shown in figure 1. The carrier concentrations vary between  $5 \times 10^{16}$  and  $1 \times 10^{19} \text{ cm}^{-3}$ . Good linearity is observed between the carrier concentration and the flow rate of disilane. There is a discrepancy in doping efficiency between the use of disilane and silane. One can tentatively attribute the discrepancy to certain native defects compensating the deliberately introduced donors, while the generation of defects depends on the growth condition. In addition, no saturation of carrier concentration was observed for relatively large concentrations in contrast to the case for disilane doping of GaAs and GaInP [48, 49]. Self-compensation of Si has been postulated as the cause of the saturation observed in GaAs [50], and one can tentatively conclude that this self-compensation does not occur in GaN. Therefore, there may be substantial differences in the Si incorporation mechanism between GaN and GaAs. As shown in figure 1, the incorporation of Si in GaN is limited by the supply of the disilane flow, and a high degree of controllability of the doping by the disilane flow rate can be readily achieved. The activation efficiency of Si dopants increases

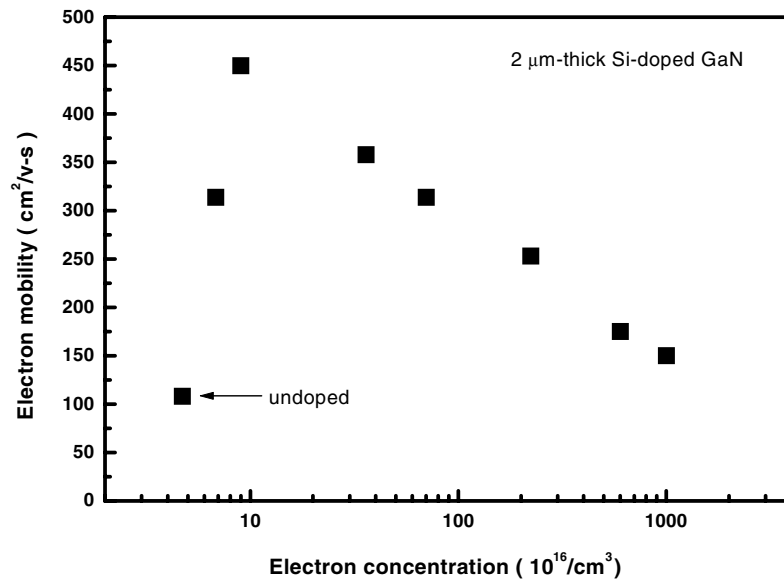


Figure 2. The dependence of the Hall mobility on the electron concentration measured at 300 K.

with increase of the Si concentration. The activation efficiency is high at higher doping levels because a so-called ‘impurity band’ is formed at high doping levels which decreases the donor ionization energy. However, Gotz *et al* [12] reported that the Si ionization energy is small enough for there to be complete ionization at room temperature, regardless of the doping level. Figure 2 shows the Hall mobility of n-type GaN as a function of the electron concentration measured at room temperature (RT). The room temperature mobility reported by Nakamura *et al* [8] is  $600 \text{ cm}^2 \text{ V}^{-1} \text{ s}^{-1}$  at a carrier concentration of  $5 \times 10^{16} \text{ cm}^{-3}$ . The mobility decreases with increase of the carrier concentration and goes down to about  $100 \text{ cm}^2 \text{ V}^{-1} \text{ s}^{-1}$  for a carrier concentration of  $1 \times 10^{19} \text{ cm}^{-3}$ . In a report, Nakamura *et al* [51] also demonstrated a highest value of electron mobility of  $900 \text{ cm}^2 \text{ V}^{-1} \text{ s}^{-1}$  at a carrier concentration of  $3 \times 10^{16} \text{ cm}^{-3}$ . In figure 2, when the electron concentrations are higher than  $1 \times 10^{17} \text{ cm}^{-3}$ , the electron mobility decreases with increase of the electron concentration. The reason for the decrease of the electron mobility is that the probability of ionized Si impurity scattering increases with increase of the electron concentration (i.e., Si concentration). In addition, it can be seen that light Si doping can enhance the Hall mobility, as shown in figure 2. As is generally known, Hall mobility strongly depends on grown-in defects. The defects can be compensatory and reduce the Hall mobility due to the scattering effect. For highly compensated undoped GaN films, the Hall mobility decreases with decreasing temperature. In a moderately doped semiconductor, mobility first increases and reaches a maximum as the temperature decreases; this corresponds to the lattice scattering limitation. When the temperature decreases continuously, the mobility declines, because of enhanced impurity scattering. A model involving transport in both the defect centres and the conduction band can be introduced to explain this phenomenon [52,53]. The transport in the defect centres may be either diffusive, due to the small but finite overlap of the localized electron wavefunctions of the defect centres, or hopping. The defect band mobility is expected to be smaller than the conduction band mobility. It is considered that the defect band conduction will be dominant when the carrier content in the conduction band becomes negligible, such as in highly resistive unintentionally doped GaN. As shown in figure 2,

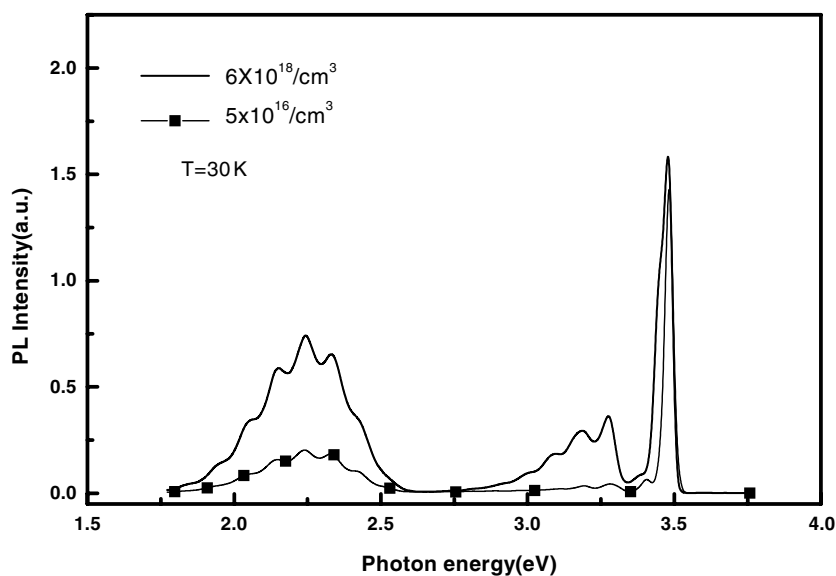
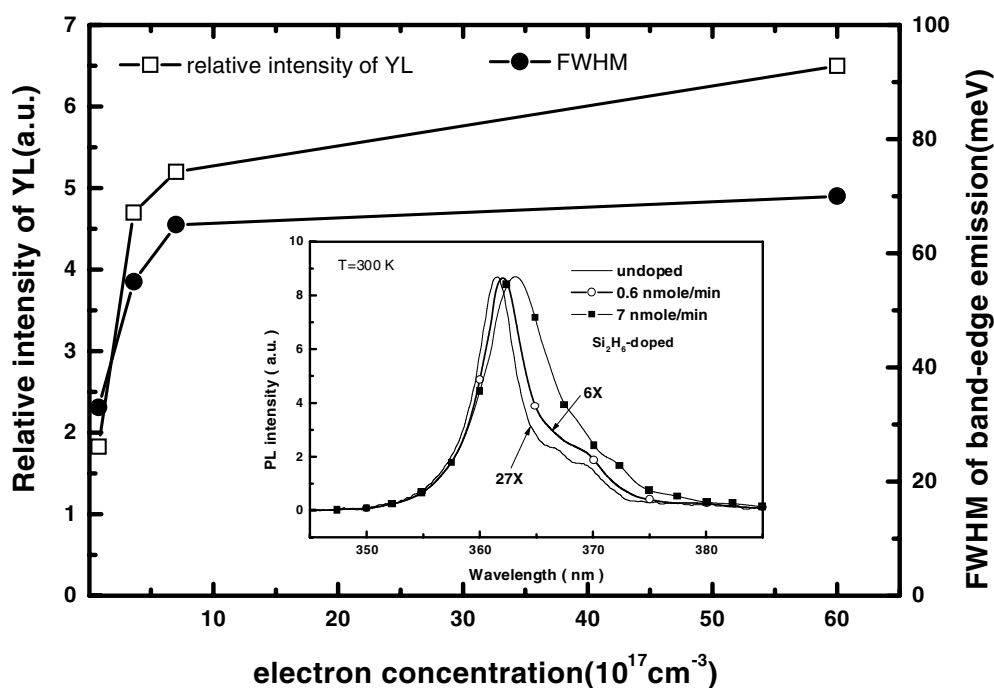


Figure 3. Typical PL spectra of Si-doped (using  $\text{Si}_2\text{H}_6$  as the doping precursor) GaN films.

Si doping can enhance the Hall mobility when the carrier concentration is below  $3 \times 10^{17} \text{ cm}^{-3}$ . It might be assumed that if the concentration of conduction donors is lower than that of deep defects (especially for unintentionally doped GaN), the material will be fully compensated, with its Fermi level pinned by these defects. In such a material, transport is dominated by hopping in the compensating centres leading to low Hall mobility. That is, deep compensatory defects as well as shallow donor (i.e. autodoping) centres coexist in the unintentionally doped GaN films. When the concentration of the shallow donor centres becomes smaller than that of the deep compensating defects, the material becomes highly resistive and transport is dominated by electron hopping through the deep compensating centres. Thus, Si doping can be expected to increase the electron concentration in the conduction band, and conduction in the conduction band to dominate the transport of carriers, leading to enhancement of the Hall mobility.

Figure 3 shows typical PL spectra, measured at 30 K, of Si-doped GaN films, whose carrier concentrations are (a)  $5 \times 10^{16} \text{ cm}^{-3}$  and (b)  $6 \times 10^{18} \text{ cm}^{-3}$  [54]. The PL spectra of the Si-doped GaN films exhibit recombination of bound excitons with neutral Si donors (band-edge emission) and intense yellow luminescence (YL) appearing at around 3.48 and 2.2 eV, respectively. For the YL band, the oscillations are attributed to the Fabry–Perot cavity formed by the air–GaN and GaN–sapphire interfaces. It is seen that the surface of the Si-doped GaN film is smooth and has a flat interface even if the carrier concentration is as high as  $6 \times 10^{18} \text{ cm}^{-3}$  due to high level of Si doping. Each deep-level peak consists of a zero-order phonon peak at about 378 nm (3.28 eV) and two LO phonon replicas at 390 nm (3.18 eV) and 402 nm (3.08 eV). The zero-order phonon peak at 3.27 eV was also observed in some undoped and lightly Mg-doped GaN films [55]. The origin of this emission line is still under debate. It may be tentatively suggested that the 3.27 eV emission line for Si-doped GaN might be due to Mg or C contamination.

Figure 4 shows the variation of the FWHM (band-edge emission) for PL spectra, measured at 30 K, with the carrier concentration, for Si-doped GaN films [54]. Note that these Si-doped GaN films were grown by MOVPE using  $\text{Si}_2\text{H}_6$  as doping precursor. It can be seen that the linewidth of the band-edge transition increases from 33 to 70 meV as the carrier concentration



**Figure 4.** The FWHM of the band-edge emission and the relative intensity of the yellow luminescence emission for  $\text{Si}_2\text{H}_6$ -doped GaN films as functions of the electron concentrations.

increases from  $5 \times 10^{16}$  to  $6 \times 10^{18} \text{ cm}^{-3}$ . The peak energy of the band-edge emission decreases with increasing  $\text{Si}_2\text{H}_6$  flow rate (i.e. carrier concentration). The decrease of the PL energy was attributed to the strain relation [66]. The broadening of this line at high carrier concentration could be attributed to tailing off of the density of states caused by potential fluctuations due to randomly distributed impurities [67, 70]. Similar phenomena were also found by Iliopoulos *et al* [65] for Si-doped GaN grown by plasma-assisted MBE. In addition, the integrated intensities of the YL calculated from the PL spectra are also shown in figure 4. The relative intensity of the YL increases with increasing carrier concentration. Recently, it was reported that the YL is due to a transition involving a complex consisting of a Ga vacancy ( $V_{\text{Ga}}$ ) and a C on a nitrogen site ( $C_{\text{N}}$ ; i.e.  $V_{\text{Ga}}\text{-}C_{\text{N}}$ ) [71]. Neugebauer and Van de Walle [8, 72] proposed that the Ga vacancy is responsible for the YL. Some experimental results also showed that the YL band was apparently suppressed by Mg-doped or Ga-rich growth conditions.  $V_{\text{Ga}}$  as a deep acceptor has low formation energy under n-type dopant conditions. Neugebauer and Van de Walle proposed that the deep acceptor level introduced by the Ga vacancy (or related complexes) is responsible for the YL of GaN, and the formation of Ga vacancies may be enhanced by formation of complexes with donor impurities. Therefore, Si incorporation would enhance the YL intensity, because the concentration of Ga vacancies increases with formation of the energetically favourable complex,  $V_{\text{Ga}}\text{-}Si_{\text{Ga}}$  ( $Si_{\text{Ga}}$ : Si on Ga site) [23]. In addition to the formation of the complex  $V_{\text{Ga}}\text{-}Si_{\text{Ga}}$ , Neugebauer and Van de Walle also suggested that the triple acceptor of the Ga vacancy and the single substitutional donor O would form a stable  $V_{\text{Ga}}\text{-}O_{\text{N}}$  complex acting as a double acceptor with a transition energy of 1.1 eV. Consequently, the model of the  $V_{\text{Ga}}\text{-}O_{\text{N}}$  complex, along with point defect Ga vacancies, is also attributed to the YL of GaN. However, Hoffmann *et al* [73] proposed another perspective on this matter. They attributed this emission line to iron impurities.

Controllable doping of n-type GaN grown by MOVPE has been achieved in many studies over a wide range of carrier concentration from  $5 \times 10^{16}$  to  $1 \times 10^{19} \text{ cm}^{-3}$ . According to previous reports and our studies [54], disilane is also a suitable n-type dopant for use in GaN epitaxial growth. Koide *et al* [7] and Lee *et al* [10] reported that the activation efficiency of Si increases with increasing Si concentration in GaN. They attributed this doping behaviour to the impurity band formed at high doping levels, decreasing the ionization energy [11]. The activation energy of Si in GaN is 8.6 meV, as was determined by Wickenden *et al* [12] using Hall-effect measurements. However, Gotz *et al* [24] also determined the activation energy for the ionization of Si donors in GaN by means of variable-temperature Hall-effect measurements. They concluded that the Si ionization energy is in the range between 12 and 17 meV. In addition, another deeper donor was also observed in Si-doped GaN with an activation energy of  $\sim 34$  meV. They tentatively suggested that the deeper donor possibly results from oxygen substituting for nitrogen ( $\text{O}_\text{N}$ ) to act as a donor. One can attribute the range of activation energies to the different levels of donor concentration and acceptor compensation in Si-doped GaN.

Some experiments had demonstrated that alternative doping sources, such as Ge, Se, and O, are also possible n-type dopants for GaN-based materials, in addition to the commonly used silicon [8, 76–78]. The doping characteristics of Ge in GaN are similar to those for Si and have been demonstrated by Nakamura *et al* [8]. As shown in figure 1,  $\text{GeH}_4$  is ten times less efficient compared to  $\text{SiH}_4$ . Specular surfaces were obtained up to carrier concentrations of  $1 \times 10^{19} \text{ cm}^{-3}$ . Beyond this value ( $1 \times 10^{19} \text{ cm}^{-3}$ ), there are some pits on the surface of Ge-doped film. Like that of Si-doped GaN, the PL spectrum of Ge-doped film displayed a UV peak around 380 nm and a YL peak around 550 nm as well [8]. In 1995, Se-doped GaN was grown by LP-MOCVD by using  $\text{H}_2\text{Se}$  as the doping source [76]. The carrier concentrations of Se-doped GaN were up to  $1.5 \times 10^{18} \text{ cm}^{-3}$ . The growth efficiency and the atomic percentage of N in the GaN can be dramatically affected by introducing  $\text{H}_2\text{Se}$ . Also, V-shaped grooves occur on the surfaces on increasing the flow rate of  $\text{H}_2\text{Se}$ . Thus, Guo *et al* suggested that  $\text{H}_2\text{Se}$  is not a favourable n-type doping source for GaN. In a later experiment, Yi and Wessels [77] reported on Se-doped GaN grown by MOVPE using  $\text{H}_2\text{Se}$  as the doping source. The carrier concentrations were in the range of  $3 \times 10^{18}$ – $6 \times 10^{19} \text{ cm}^{-3}$ . Carrier concentration is linearly proportional to the partial pressure of  $\text{H}_2\text{Se}$  at low pressure, but a sublinear dependence on pressure was observed at high partial pressure. However, the Hall-effect measurements indicated that Se-doped GaN is highly compensated even for heavily doped material. In addition, PL measurements at 15 K also indicated a strong acceptor-related transition at 3.447 eV in the heavily doped films. According to Yi and Wessels' comments, the compensating acceptor in Se-doped GaN could be attributed to the triply charged gallium vacancy ( $\text{V}_{\text{Ga}}^{-3}$ ), which is consistent with theoretical calculations of defect stability in GaN [75].

Several SIMS studies have observed large concentrations of Si and O in unintentionally doped GaN [24–29]. di Forte-Poisson *et al* proposed that the electron concentration is directly proportional to the amount of oxygen incorporated up to a concentration level of  $3 \times 10^{19} \text{ cm}^{-3}$ . Therefore, it can be tentatively believed that O substituting for N would lead to simple shallow donors in GaN. Intentionally oxygen-doped GaN, grown by MOVPE, was first obtained by Chung and Gershenson [79]. Their data showed that the electron concentrations varied from the mid-range of  $10^{19}$  to a low  $10^{20} \text{ cm}^{-3}$ . Chung *et al* [28, 80] suggested that oxygen is a 'shallow' deep donor with an activation energy of 78 meV as determined by optical measurements from the energy of the donor bound exciton, although the nature of oxygen donor in GaN remains controversial. In some later studies, the electrical properties of both unintentionally and intentionally oxygen-doped n-type GaN were reported [27, 80, 81]. In contrast to the conclusion of Chung and Gershenson, oxygen donors are shallow, with thermal ionization energies ranging from 2 to 29 meV, which were determined by temperature-dependent Hall-effect

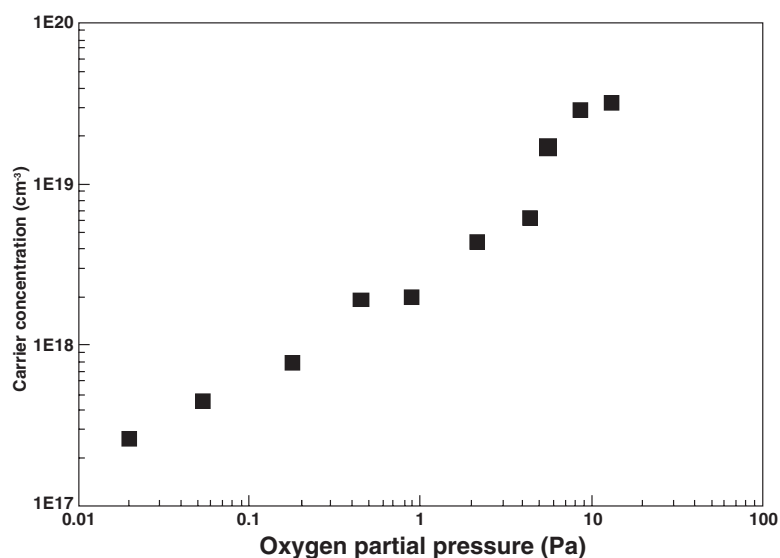


Figure 5. Carrier concentration versus O<sub>2</sub> partial pressure for oxygen-doped n-type GaN.

measurements. In addition, Niebuhr *et al* [82] employed N<sub>2</sub>O as the oxygen source to dope GaN. Their results showed that the electron concentration increased with increasing partial pressure and saturated at a level of  $4 \times 10^{18} \text{ cm}^{-3}$ . Recently, Korotkov and Wessels reported that oxygen is a simple donor in GaN and the donor activation energy is around 27 meV [78]. As shown in figure 5, O-doped GaN grown by MOVPE using oxygen–nitrogen gas as the doping source has carrier concentrations in the range of  $3 \times 10^{17}$ – $3 \times 10^{19} \text{ cm}^{-3}$  [78]. The electron concentration increase with the partial pressure of oxygen up to  $7 \times 10^{18} \text{ cm}^{-3}$ . The compensation ratio was also determined as 0.4 for electron concentration below  $8 \times 10^{18} \text{ cm}^{-3}$ . Above the value of  $8 \times 10^{18} \text{ cm}^{-3}$ , the compensation ratio varies from 0.4 to 0.6. Zolper *et al* reported directly implanting O<sup>+</sup> ions into insulating GaN, activated by annealing at 1000 °C; the activation efficiency of the implanted oxygen was as low as ~4%, but n-type GaN was created and an ionization energy of ~29 meV was measured [83]. In the light of the previous reports, it appears that the activation energy of O in GaN is similar to that of Si [12, 24, 78, 80–83]. However, the controllability of the doping level for Si in GaN should be superior to that of O.

Al<sub>x</sub>Ga<sub>1-x</sub>N has been frequently used for cladding layers of group III nitride laser diodes and light-emitting diodes. Therefore, it is necessary to be able to have n- and p-type Al<sub>x</sub>Ga<sub>1-x</sub>N layers. In early work, Khan *et al* [84] reported that unintentionally doped Al<sub>x</sub>Ga<sub>1-x</sub>N films with  $x > 0.4$  exhibit a high-resistivity characteristic. In a later report, Yoshida *et al* [85] also observed a rapid increase in the resistivity of undoped Al<sub>x</sub>Ga<sub>1-x</sub>N films with increasing Al content. Lee *et al* also showed that there is a significant increase in resistivity of Al<sub>x</sub>Ga<sub>1-x</sub>N for Al contents in the range 40–60% [86]. It was suggested that, as the Al content in Al<sub>x</sub>Ga<sub>1-x</sub>N alloy increases, the dopant moves deeper into the forbidden energy band gap. A different interpretation is that the ionization energies of native defects increase with increasing Al content in Al<sub>x</sub>Ga<sub>1-x</sub>N. More studies are needed to clarify the mechanism responsible. Bremser *et al* [87] also demonstrated the doping characteristics of Si-doped Al<sub>x</sub>Ga<sub>1-x</sub>N alloys with Al contents in the range  $0.12 < x < 0.42$ . A rapid decrease in the effective donor concentration with increasing Al content ( $x > 0.42$ ) was observed. These results indicated that the additional Si was not activated in the Al<sub>x</sub>Ga<sub>1-x</sub>N alloys. It is well known that the activation energy for

the donors increases as the Al content increases in  $\text{Al}_x\text{Ga}_{1-x}\text{N}$  alloys, because the donor states become deeper. Stampfl and Van de Walle [88] proposed that the DX transition of oxygen and compensation by the cation vacancy ( $V_{\text{Ga}}$  or  $V_{\text{Al}}$ ) are responsible for the rapid decrease in electron concentration of  $\text{Al}_x\text{Ga}_{1-x}\text{N}$  alloys with  $x > 0.4$ . However, this phenomenon was also observed for Si-doped  $\text{Al}_x\text{Ga}_{1-x}\text{N}$  alloys, and Si does not undergo a DX transition in  $\text{Al}_x\text{Ga}_{1-x}\text{N}$  alloys with increasing Al content. They proposed that the discrepancy between Si and oxygen can be comprehended on the basis of the different locations in the lattice and a Coulomb repulsion induced between ions, leading to a suppression of Si-related DX formation. But in the Si-doped  $\text{Al}_x\text{Ga}_{1-x}\text{N}$  alloy autodoping of oxygen also occurs to a great extent. The residual oxygen can still undergo the DX transition and therefore effectively becoming compensating centres. Polyakov *et al* [89] inferred the possibility that the decrease in electron concentration for high-Al-content  $\text{Al}_x\text{Ga}_{1-x}\text{N}$  alloy ( $x > 0.3$ ) may be due to the formation of oxygen DX centres, which act as negatively charged acceptors, compensating the Si-doped n-type conductivity. Also, Stampfl and Van de Walle [88] proposed that triply charged Al vacancies,  $V_{\text{Al}}^{-3}$ , are formed in the highly doped n-type  $\text{Al}_x\text{Ga}_{1-x}\text{N}$  alloys for  $x > 0.4$ . These defects compensate the n-type doping and reduce the conductivity when the dopant is Si. The conductivity decreases rapidly with increase of the Al content in  $\text{Al}_x\text{Ga}_{1-x}\text{N}$  alloys; this was also observed in undoped and Ge-doped films which were grown using ECR microwave plasma [90].

For high-efficiency light emitters, double heterostructures are required. In nitride semiconductor systems, quaternary  $\text{Al}_x\text{In}_y\text{Ga}_{1-x-y}\text{N}$  can be tailored to form heterostructures. In particular, the ternary alloy  $\text{In}_x\text{Ga}_{1-x}\text{N}$  is one possibility for use as the active layer of blue or green emitters. Yoshimoto *et al* [91, 92] showed the effect of growth conditions on the carrier concentration and transport properties of  $\text{In}_x\text{Ga}_{1-x}\text{N}$ . They revealed that if the growth temperature of  $\text{In}_x\text{Ga}_{1-x}\text{N}$  ( $x \approx 0.2$ ) is increased from 500 to 900 °C, the carrier concentration will reduce from  $10^{20}$  to  $10^{18} \text{ cm}^{-3}$ . The mobility will also increase from  $<10$  to  $100 \text{ cm}^2 \text{ V}^{-1} \text{ s}^{-1}$  if the growth temperature is increased from 500 to 900 °C. On the other hand, Abernathy *et al* [93] also reported that the electron concentration of undoped InN gradually decreases with increasing growth temperature. One can assume the quality of the  $\text{In}_x\text{Ga}_{1-x}\text{N}$  epilayers to be improved by the elevated growth temperatures. Therefore, the background carrier concentration decreases and the mobility increases.

As is generally known, unintentionally doped InN is heavily n-type ( $n > 10^{20} \text{ cm}^{-3}$ ), regardless of the growth technique [94], and this is usually ascribed to the presence of In vacancies [126, 233]. Considering the results of ion channelling and Auger electron analysis, which indicated a stoichiometric or slightly nitrogen-rich composition, Abernathy *et al* [93] suggested that native defects rather than  $V_{\text{N}}$  or impurities are responsible for the residual doping in  $\text{In}_x\text{Ga}_{1-x}\text{N}$  films. In other words, they suggested that impurities such as oxygen or carbon are responsible for the strongly n-type conductivity of InN even in high-In-content  $\text{In}_x\text{Ga}_{1-x}\text{N}$  films. Intentionally doped  $\text{In}_x\text{Ga}_{1-x}\text{N}$  films have been demonstrated by Nakamura *et al* [96, 97], which the dopants are Si, Cd and Zn. Nakamura *et al* [98] reported that the PL peak of  $\text{In}_{0.14}\text{Ga}_{0.86}\text{N}$  is not changed by Si incorporation during growth, but the PL intensity becomes much stronger than that of undoped film. In addition, they also demonstrated that the PL intensity of the Cd-related emission was almost the same as that of the band-edge emission of Si-doped InGaN. In contrast to the case for Si-doped InGaN, the blue emission peak wavelength is at an energy level 0.5 eV lower than the band-gap energy of InGaN [98]. The 0.5 eV difference between Cd-related emission and band-edge emission energies is similar to that for Cd-doped GaN films [99]. On the other hand, Zn-doped InGaN films with strong blue emission were also demonstrated by Nakamura *et al*; the Zn-related emission energy is always about 0.5 eV lower than the band-edge emission energy of undoped or Si-doped

InGaN [98]. They also reported that the PL intensity of  $\text{In}_{0.23}\text{Ga}_{0.77}\text{N}$  films codoped with Si and Zn exhibited a dependency on the carrier concentration (n-type). For carrier concentrations of codoped InGaN below  $1 \times 10^{19} \text{ cm}^{-3}$ , the PL intensity decreases with decreasing carrier concentration, and the peak energy shifts from blue emission at low Zn concentration to red at high Zn concentration [67, 100]. In the light of this deep-level nature of Zn in InGaN, the early double-heterostructure blue LEDs were fabricated by using a Zn/Si-codoped InGaN active layer to shift the emission peak from the near ultraviolet to blue or green [98].

Silicon doping of InGaN well and barrier layers has also been reported to improve the device characteristics, such as threshold current and voltage, of laser diodes [101]. The effect may be attributed to improved structural perfection or the built-in polarization field screening, resulting in higher emission efficiencies of quantum wells (QWs) [102–106]. Some results on the structural quality of MQWs as a function of Si doping level were derived from the linewidth broadening effect of the higher-order superlattice satellite peaks measured using XRD. In addition, PL and PLE measurements reveal a decrease in the Stokes shift with increasing Si doping level. On the other hand, the radiative recombination lifetime was observed to decrease from  $\sim 30$  to  $\sim 4$  ns as the Si doping level increased from  $n \sim 1 \times 10^{17}$  to  $3 \times 10^{19} \text{ cm}^{-3}$ . Cho *et al* [106] also concluded that the reduced Stokes shift, the decrease in radiative recombination lifetime, and the increase in interface quality are due to decreases in carrier localization at potential fluctuations in the Si-doped InGaN active layer. It is generally known that  $\text{In}_x\text{Ga}_{1-x}\text{N}/\text{GaN}$  QW structures are grown at lower temperature than GaN in order to optimize the growth of the  $\text{In}_x\text{Ga}_{1-x}\text{N}$  well. However, this temperature is too low for growing high-quality GaN barriers. Recently, Keller *et al* [107] showed that undoped GaN barriers grown at low temperature form island-like spiral structures initiated by threading dislocations that exist in the underlying template GaN layer; but formation of the spiral structure is dramatically suppressed by Si doping during the growth of the GaN barrier even at low temperature. Similar results were also observed for the  $\text{Al}_x\text{Ga}_{1-x}\text{N}/\text{GaN}$  QW, in which Si doping significantly improved the crystalline quality of MQWs [108]. Generally, MQWs with high optical and/or electrical qualities can be achieved with well thicknesses below the critical thickness. When the well width exceeds the critical thickness, high-density misfit dislocations will be generated and these defects degrade the quality of QWs. It has been reported that Si doping decreases dislocation density and hence improves the crystalline quality of GaN layers too [109].

### 3.2. p-type materials

**3.2.1. GaN.** One of the many challenges associated with the development of III–V nitride materials is the control and understanding of their electrical behaviours. In most cases, the unintentionally doped group III nitride materials are n-type. However, under appropriate growth conditions, this residual doping can be reduced to levels low enough to allow controllable doping, both n-type and p-type. The case of p-type doping in GaN is much more complicated than that of n-type doping. In addition, bonding energies of dopants depend on the dielectric constant (GaN,  $\epsilon_r = 9.5$ ) and effective mass (GaN,  $m_e = 0.2 m_0$ ,  $m_{hh} = 0.75 m_0$ ). Both factors are large for GaN; thus the bonding energies of the dopants are larger. For p-type doping, the acceptor level of GaN is deeper than the GaAs acceptor level due to its larger hole mass. This leads to the difficulty in p-type doping and very low activation of dopants at room temperature for GaN.

The most widely used dopant for p-type GaN is magnesium. No other impurity has been so successful in producing p-type conductivity in GaN. Generally, Mg-doped GaN grown by MOVPE exhibits the semi-insulating property. It was thought that hydrogen behaves as a

donor ( $H^+$ ) compensating acceptors (Mg), which forms the neutral complexes Mg–H [111]. Amano *et al* [2] achieved p-type GaN films by using a LEEBI treatment after the growth. This treatment converts semi-insulating Mg-doped GaN into conductive p-type material [2]. The effect of the LEEBI treatment was assumed to provide the energy to displace Mg to the Ga lattice site, which activates the Mg to be an acceptor in GaN. In 1991, Nakamura *et al* [3] showed that low-resistivity p-type GaN films can be obtained by thermal annealing at temperatures around 700 °C in an  $N_2$  ambient. In addition, Nakamura *et al* also demonstrated that significant increases of resistivity occurred as LEEBI-treated p-type GaN films were annealed in an  $NH_3$  ambient. They concluded that atomic hydrogen generated by  $NH_3$  dissociation was responsible for the passivation of acceptors. The role of hydrogen atoms in the mechanism of passivation of the Mg acceptors in GaN was then clarified for the first time [3]. This correlation between hydrogen and magnesium concentrations was further elucidated by Ohba and Hatano [112]. Due to this passivation effect, as-grown Mg-doped GaN requires post-growth heat treatment to activate the dopants. Interstitial hydrogen is incorporated and the Mg–H complex is formed; these passivate the acceptor during the MOVPE growth. This Mg–H bond can be broken by a high-temperature annealing step in an inert-gas environment. Undoubtedly, the thermal annealing technique represents a breakthrough in obtaining p-type III–V nitride films, because it is an easy, reliable, and mass-production process. In addition, it can be effected *in situ* in the MOVPE system. On the other hand, only a thin layer is really activated by using the LEEBI treatment, since low-energy electrons have a small penetration depth in GaN. Thus, the thermal annealing technique is commonly used to obtain p-type versions of GaN films which were grown by MOVPE. Recently, a microwave treatment method, which is different from thermal annealing and LEEBI, was proposed to activate Mg dopants in p-type GaN epitaxial layers [168]. Considering the PL spectra and the Hall-effect measurements, the activation of Mg dopant in p-type GaN layers may be explained as the breaking of magnesium–hydrogen bonds due to the microwave energy absorption. In addition, Lai *et al* [169] used a  $CO_2$  laser to perform acceptor activation of Mg-doped GaN in air. They suggested that laser irradiation was absorbed by GaN and sapphire, thereby heating the GaN film. Consequently, results obtained from  $CO_2$  laser treatment are similar to those from thermal annealing or LEEBI treatment to convert the highly resistive Mg-doped GaN into low-resistivity p-type GaN. Takeya and Ikeda [170] had also demonstrated two methods for p-type activation of Mg-doped GaN. One is low-temperature and long-time thermal annealing in air. This process was performed at 385 °C; the hole concentration obtained was up to  $1 \times 10^{18} \text{ cm}^{-3}$  after 80 h of annealing. They reported that Arrhenius analysis yields an activation energy of  $\sim 1.7 \text{ eV}$  in this process. This value is close to the theoretically calculated value of the M–H dissociation energy of  $\sim 1.5 \text{ eV}$  [111]. In the second activation method, Mg-doped samples were placed between RF electrodes which work at 13.56 MHz under a chamber pressure of  $10^{-5}$  Torr in order to prevent the generation of plasma. In the case of RF activation, the heating temperature was 300 °C and the hole concentration increased with RF exposure time. Takeya *et al* [111] tentatively concluded that this activation process is the accelerated electron attack on Mg–H bonds and/or energy absorption of the Mg–H complexes itself, occurring because of polarization. Another possible mechanism was also proposed: the enhancement of hydrogen out-diffusion by the RF electric field, since atomic hydrogen is most stable in the ionization state in GaN. However, the typical hole concentration in Mg-doped GaN is below  $1 \times 10^{18} \text{ cm}^{-3}$ . Thus, the activation efficiency of Mg is lower than 10% in GaN. Achieving a high hole concentration with Mg as the dopant is still not an easy task. Neugebauer and Van de Walle [115] commented that the determining factor is the solubility of magnesium in GaN, which is limited by competition between incorporation of Mg atoms and formation of  $Mg_3N_2$ . In addition, in the presence of H, the Mg atoms are passivated. Consequently, different complexes such as  $Mg_{Ga}\text{--}N\text{--}H$ ,

$\text{Mg}_i\text{H}_2$ ,  $\text{Mg-N-Ga-H}_2$ , and  $\text{Mg}_{\text{Ga}}\text{-N-Mg}_i\text{-H}$  are likely to form and Mg acceptors will become electrically inactive [116]. Although it has been frequently mentioned that Mg and H form a complex in Mg-doped GaN films, Van Vechten *et al* [117] and Neugebauer and Van de Walle [75, 111, 118] suggested that hydrogen is beneficial to p-type doping with Mg when compared to the hydrogen-free case. They proposed that the hydrogen passivates the Mg during growth, therefore repressing the formation of native donors to compensate the acceptors. For the MOVPE case, it has been argued that H is in a positive charge state and passivates the Mg acceptors, which are in their negative charge state during growth; this would prevent the Mg from being compensated by donor-like defects, such as the nitrogen vacancy ( $\text{V}_{\text{N}}^+$ ) and interstitial gallium ( $\text{Ga}_i^{3+}$ ) [30].  $\text{V}_{\text{N}}^+$  and  $\text{Ga}_i^{3+}$  both have low formation energies in p-type material [30]. On the other hand, it was predicted that more magnesium would be incorporated into a GaN film when there are more hydrogen atoms present. In other words, an H-rich environment can repress the formation of  $\text{Mg}_3\text{N}_2$  during growth. H passivates substitutional Mg ( $\text{Mg}_{\text{Ga}}^-$ ) by forming an  $\text{Mg}_{\text{Ga}}\text{-N-H}$  complex [24, 73, 74]. The Fermi level then rises to the mid-gap region and the formation energies of  $\text{V}_{\text{N}}^+$  and  $\text{Ga}_i^{3+}$  are increased. Although the H-rich environment will produce more Mg-H-related complexes to passivate the Mg acceptors, low-resistivity p-type GaN would be obtained due to the eviction of  $\text{H}^+$  by the post-growth annealing and thereby generate negatively charged Mg acceptors. Despite hydrogen passivation during the growth of nitride semiconductors seeming inevitable, *in situ* p-type conductivity for Mg-doped GaN films grown by a reactive molecular-beam epitaxy (MBE) technique which employs ammonia as the nitrogen source has been reported [119]. After thermal annealing in nitrogen ambient, no noticeable influence on the electrical properties of the films could be detected. More than 6% of incorporated Mg atoms were activated for the as-grown samples with relatively low Mg concentrations. In a later study, Sugiura *et al* [120] reported that low-resistivity *in situ* p-type GaN can be obtained by  $\text{N}_2$ -ambient MOVPE growth. Contesting the general view, they concluded that hole compensation caused by hydrogen passivation is not an obstacle to achieving low-resistivity p-type GaN in  $\text{N}_2$ -ambient MOVPE growth; *in situ* p-type GaN can be realized by  $\text{H}_2$ -free growth and the hole concentration can be as high as  $1 \times 10^{18} \text{ cm}^{-3}$ . They also clarified that hydrogen generated by  $\text{NH}_3$  dissociation does not prevent Mg from being electrically activated under  $\text{H}_2$ -free growth conditions; this result is similar to the situation for Mg-doped p-type GaN grown by reactive MBE [119]. However, in the light of their comments, it seems that the small amount of  $\text{H}_2$  carrier gas will strongly influence the electrical properties of Mg-doped GaN films.

Figure 6 shows the hole concentration and FWHM of (0004) x-ray diffraction of Mg-doped GaN grown by MOVPE as functions of  $\text{CP}_2\text{Mg}$  flow rate [121]. The maximum hole concentration of  $6 \times 10^{17} \text{ cm}^{-3}$  was obtained at a flow rate of  $0.9 \mu\text{M min}^{-1}$ , as shown in figure 6. The hole concentrations of the Mg-doped GaN films decrease with increase of  $\text{CP}_2\text{Mg}$  flow rate when the flow rates are higher than  $0.9 \mu\text{M min}^{-1}$ . Surprisingly, the hole concentrations of the Mg-doped GaN films are less than or equal to  $1 \times 10^{17} \text{ cm}^{-3}$  when the  $\text{CP}_2\text{Mg}$  flow rate is lower than  $0.6 \mu\text{M min}^{-1}$ . This could be attributed to only a few Mg atoms acting as acceptors to compensate the native donors (defect or impurity related), and thus the films showing lower hole concentration. Quantitative estimates of Mg concentrations, determined by SIMS measurements, are not available among the above-mentioned results, so we cannot precisely calculate the solid-vapour ratio for magnesium in GaN. However, the incorporation of magnesium can be expected to be proportional to the  $\text{CP}_2\text{Mg}$  molar flow rate. This expectation might be (tentatively) proved by the FWHM of the x-ray diffraction spectra, as shown in figure 6. It can be seen that the FWHM of the x-ray diffraction increased with increasing  $\text{CP}_2\text{Mg}$  flow rate. Since magnesium has a larger radius than gallium, it may be incorporated as a substitutional and/or interstitial. Thus, we may anticipate that high

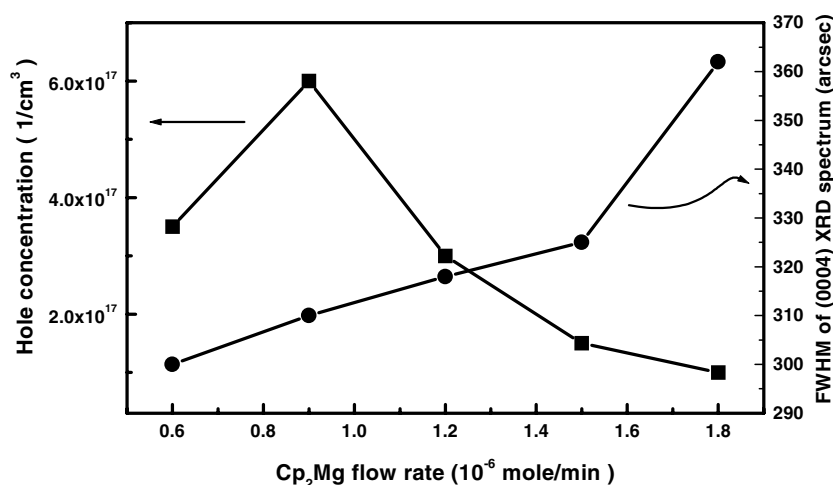


**Figure 6.** The hole concentration and FWHM for (0004) x-ray diffraction of Mg-doped GaN as functions of  $\text{CP}_2\text{Mg}$  flow rate.

magnesium concentrations will degrade the crystal quality of GaN. In fact, the morphology of Mg-doped GaN is specular when the  $\text{CP}_2\text{Mg}$  flow rates are below  $1.5 \mu\text{M min}^{-1}$ , but cracks and/or hexagonal pyramids occur at higher  $\text{CP}_2\text{Mg}$  flow rates, as shown in figure 7.

At this point, it is not clear why the hole concentration decreased as the  $\text{CP}_2\text{Mg}$  flow rate (Mg concentration) increased. A similar result was also reported by Bour *et al* [122, 175]. Neugebauer and Van de Walle [75, 111, 118] suggested that the incorporation of Mg at substitutional nitrogen sites or at interstitial sites should be the cause of the limited doping efficiency. One can attempt to interpret this phenomenon by suggesting that the incorporated Mg atoms may not only choose to occupy Ga sites, since a reasonable crystalline quality with higher Mg concentration (high  $\text{CP}_2\text{Mg}$  flow rate) cannot be maintained. In other words, one does not exclude the possibility of the presence of Mg atoms at interstitial sites rather than Ga sites or the formation of the nearest-neighbour pair  $\text{Mg}_{\text{Ga}}\text{V}_{\text{N}}$ , a double donor. These might induce negative charged defects, thereby compensating the holes. Therefore, achieving a high hole concentration with Mg as the dopant is difficult even though it is possible to increase the Mg concentration; the hole concentration could level off, and even decrease [122]. On the other hand, Kaufmann *et al* [123] also commented that the limited p-type conductivity in MOVPE-grown Mg-doped GaN might be attributed to self-compensation by intrinsic lattice defects such as vacancies or interstitial host atoms ( $\text{Mg}_i$ ) rather than donor impurity background compensation, especially for those GaN samples with high Mg concentration.

Despite many significant technological breakthroughs, such as the development of high-brightness light-emitting diodes and violet laser diodes, many properties of this material system are not well understood. Various potential p-type dopants have been incorporated into GaN since the early 1970s [126]. The optical properties of Mg-doped GaN, which was grown by MOVPE with  $\text{CP}_2\text{Mg}$  as the precursor, were first demonstrated by Amano *et al* [2]. They found that, at low temperature (4.2 K), samples with low Mg concentration exhibit a PL peak at 3.27 eV and its LO phonon replicas, indicating that Mg acts as an acceptor. In a later report, Nakamura *et al* [127] also reported that the PL spectra, at room temperature, of Mg-doped GaN films show a strong peak at around 2.8 eV. The PL spectrum of Mg-doped GaN exhibits an emission peak that shifts from 3.21 eV at 150 K [128] to 3.18 eV at 6 K [129].

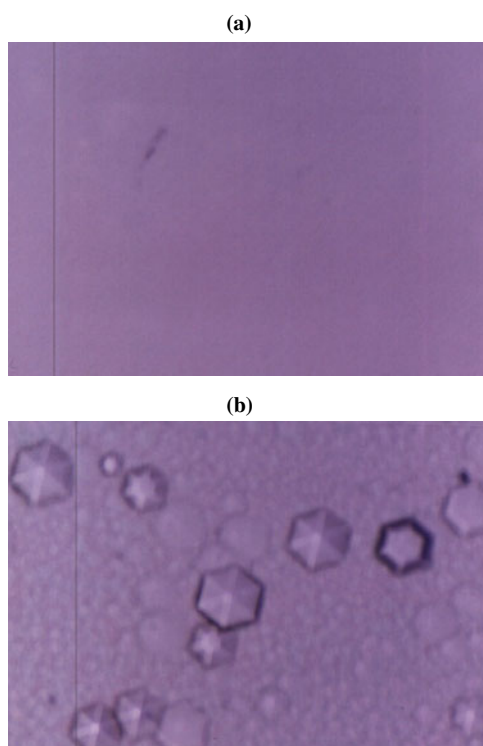


**Figure 7.** Surfaces of Mg-doped GaN films which were grown under the same conditions except as regards the  $\text{CP}_2\text{Mg}$  flow rate: (a)  $0.9 \mu\text{M min}^{-1}$  and (b)  $3 \mu\text{M min}^{-1}$ .  
(This figure is in colour only in the electronic version)

It was assigned to a transition from a conduction band to a shallow Mg-related acceptor level rather than the donor–acceptor-pair (DAP) transition. However, the 3.2–3.3 eV emission line (at 20 K) for Mg-doped GaN has been reported by Strite and Morkoc [129] and Hong *et al* [130]. They assigned the emission line to the DAP transition. The Mg-related DAP transition in GaN was first reported by Dingle and Ilegems in 1971 [131]. Usually, the mechanisms of the DAP transitions in semiconductors are studied by using excitation intensity-resolved PL measurements [139]. Figure 8 shows typical PL spectra of Mg-doped GaN (with a hole concentration of  $3 \times 10^{17} \text{ cm}^{-3}$ ) taken at 20 K. There are two dominant emission peaks from 2.86 to 2.95 eV at which the excitation energy increases [139]. In the 20 K PL spectra of Mg-doped GaN, the emission peak at around 3.2 eV, which was reported by other authors [128, 135], is not observed. As shown in figure 8, the line shape of the emission band depends on the laser power density. This is a distinctive characteristic feature of the DAP transition in semiconductors [137]. The emission peaks around 2.95 eV and 2.86 eV can be attributed to the DAP transition [134, 138–140]. A considerable Coulomb broadening of the DAP luminescence, with FWHM ranging from 180 to 290 meV, is also displayed in figure 8. At higher excitation power, the band fluctuations are gradually screened by light-induced electrons, and holes then remove the band fluctuation and therefore reduce the bandwidth. This result indicates that the dominant emission band shifts toward higher energy (around 2.95 eV) as the excitation intensity is increased. A similar phenomenon was also observed in InGaN/AlGaN double-heterostructure light-emitting diodes with the InGaN

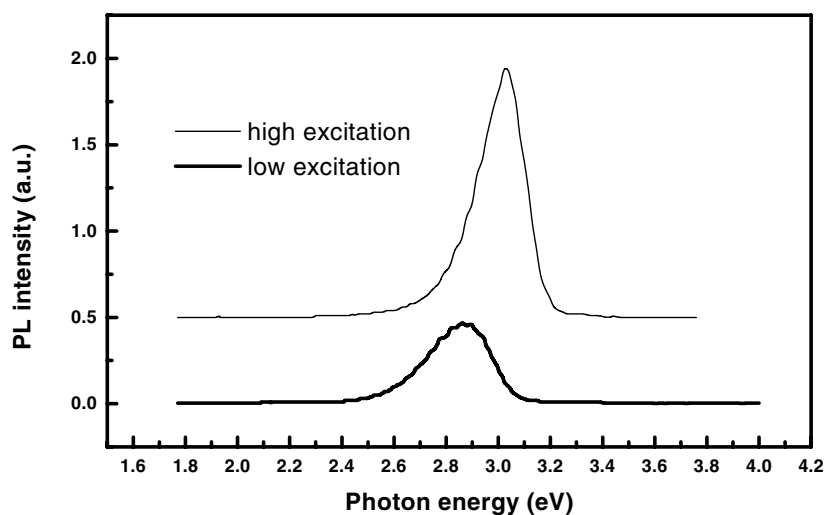
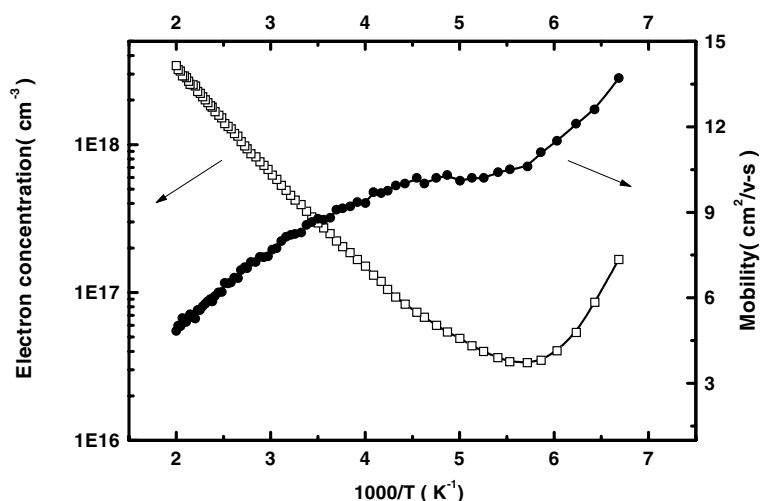


Figure 8. Typical PL spectra of Mg-doped GaN at a temperature of 20 K.

active layer codoped with Si and Zn [142]. Casey *et al* [142] ascribed the blue-shift to the band-filling mechanism. For the process of band filling, the shift in the emission peak results from injected minority carriers filling the empty acceptor levels and the valence band tails in the codoped layer and therefore compensating the active layer. This emission line in Mg-doped GaN, around 2.95 eV, can be attributed to the transition between the deep levels of native or impurity-related donors [30, 75] and the Mg-related acceptor level which is 160–250 meV above the valence band [143]. This result is different from the previously published results, where the emission line at 2.95 eV was assigned to the transition from the conduction band to the doping-related deep-level impurity [128–130]. On the other hand, the discrepancy between these reports, based on time resolution and the excitation density dependence of the PL spectra, may be ascribed to different doping levels of Mg-doped films. It can be suggested that for some highly compensated Mg-doped GaN films, the donor states will merge with the conduction band and the free-electron–acceptor transition will be dominant in the PL spectra. It is well known for GaAs with different doping levels that the luminescence energy associated with the DAP transition is red-shifted with increasing doping concentration. This has also been interpreted using a model in which a fluctuating potential affects the bands and impurity levels [141]. For lower doping levels, the potential fluctuation depth will be small. Thus, the DAP transition peak is at higher energy for samples with lower doping concentrations and does not significantly shift with increasing excitation density. In contrast, for higher doping levels, the DAP transition peak is at a lower energy and will be significantly shifted with increasing excitation density.

It is well known that acceptor dopants, such as Mg, Be [144–148], Zn [149–151], and C [152–155], have high ionization energies in GaN-based materials. Mg-doped p-type GaN play a critical role for a host of nitride-based optoelectronic devices [1]. Because of the deep nature of the Mg acceptor, very high doping levels of  $\sim 10^{19} \text{ cm}^{-3}$  are frequently used in device applications. However, hole concentrations are obtained for Mg-doped GaN in the middle of the  $10^{17} \text{ cm}^{-3}$  region. Therefore, only a few per cent of the Mg atoms are ionized at room temperature. Temperature-dependent Hall-effect measurements have been performed on Mg-doped GaN; activation energies for substitutional  $\text{Mg}_{\text{Ga}}$  acceptors ranging from 112 to 210 meV were reported [31, 119, 156, 157]. Figure 9 shows the temperature-dependent Hall



**Figure 9.** Temperature-dependent Hall measurements of Mg-doped p-type GaN which had been annealed in nitrogen at 700 °C for 30 min.

measurements of Mg-doped p-type GaN which had been annealed in nitrogen at 700 °C for 30 min. The hole concentrations decrease from  $\sim 3 \times 10^{18}$  to  $\sim 3 \times 10^{16}$  cm $^{-3}$  as temperature decreases from 500 to 180 K. An effective activation energy of around 140 meV is extracted from the Arrhenius plot in this temperature range. At lower temperature ( $T < 180$  K), the hole concentrations increase again. This transport process could be attributed to the onset of impurity band conduction where carriers can propagate within the impurity band without entering the valence band [158]. Therefore, in the low-temperature region, the one-carrier analysis method used for calculating the actual hole concentrations may be invalid.

Tanaka *et al* [157] reported two activation energies, 125 and 157 meV, from Hall-effect measurements of samples grown by MOVPE. Huang *et al* [159] showed an activation energy of 136 meV in MOVPE-grown samples with a high hole concentration in Mg-doped GaN. According to the results of Hall-effect measurements, Johnson *et al* reported an activation energy of 170–182 meV for MOCVD-grown Mg-doped samples, while a lower value was obtained from dark-current measurements, about 131 meV [160]. Considering the activation energy of Mg in GaN, no coherent picture of the acceptor levels can be obtained from the reported literature. Seghier and Gislason [161] reported that there may be two acceptor levels, at  $E_v + 130$  meV and  $E_v + 170$  meV, in Mg-doped GaN. The number of acceptors with the energy level 130 meV above the valence band increases with increase of the hole concentration, and increases with annealing time. In addition, according to the results of thermally stimulated current (TSC) measurements, only the  $E_v + 170$  meV acceptor level is electrically active in the as-grown samples. Thus, Seghier and Gislason suggested that the compensation mechanism in as-grown Mg-doped GaN is related to the passivation of the acceptor level at  $E_v + 130$  meV, which controls the conductivity in the annealed samples. Undoubtedly,  $N_2$ -ambient thermal annealing is the most common and most reliable method for activating Mg-doped GaN. It is suggested that Mg–H complexes are responsible for the high resistivity in as-grown Mg-doped GaN [3, 162, 163]. Nakamura *et al* have shown that a post-growth heat treatment in  $N_2$  causes the Mg–H complexes to dissociate and results in H out-diffusion from the GaN layer and activation of the Mg dopants. Recently, it has been shown that the presence of oxygen in the annealing environment can have a dramatic effect on the activation [163, 164].

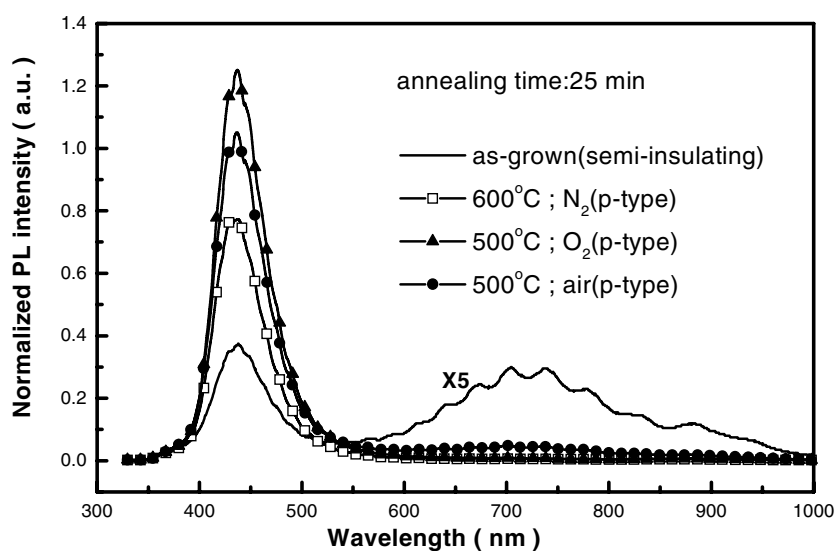


**Figure 10.** Room temperature PL spectra of Mg-doped GaN for various annealing ambients (exposure for 25 min) [54].

Ho *et al* [165] demonstrated a specific contact resistivity ( $\rho_c$ ) of  $4 \times 10^{-6} \Omega \text{ cm}^{-2}$  when the Ni/Au contacts were annealed at  $500^\circ\text{C}$  in air. Chen *et al* [166] and Ho *et al* concluded that the formation of NiO islands in contact with the p-type GaN surface during the heat treatment in air is responsible for this striking result. Koide *et al* [164] have also reported that better ohmic contacts and lower sheet resistance of the p-type GaN can be achieved by alloying p-type GaN/Ni/Au contacts in  $\text{O}_2$ -containing ambient at  $500\text{--}600^\circ\text{C}$ . However, they concluded that the reduced  $\rho_c$  could be attributed to the enhanced dissociation of residual Mg–H complexes during the  $\text{O}_2$ -containing-ambient annealing process. In other words, the Mg acceptors in films were further activated during contact annealing processes. Therefore, one can assume that the moderate oxygen level is conducive to activation of p-type GaN. Figure 10 shows room temperature PL spectra of Mg-doped GaN samples which were annealed in different ambients such as  $\text{N}_2$ ,  $\text{O}_2$ , and air [54]. As shown in figure 10, before thermal annealing, the intensity of the typical blue emission at  $440 \pm 5 \text{ nm}$  is very weak and the broad deep-level emission can be observed at around  $750 \text{ nm}$  (deep-level emission). It can be seen that upon thermal annealing in various gas ambients, the blue band becomes intense and the deep-level emission disappears. The use of oxygen annealing seems to produce the best results. The PL intensities of  $\text{O}_2$ -annealed samples at  $500^\circ\text{C}$  are ten times larger than that for the as-grown sample. This implies that the oxygen plays an important role in the activation of Mg in MOVPE-grown GaN. Resistivities of p-type GaN films are shown in figure 11 as functions of annealing temperature. The annealing time was 25 min. The resistivities were obtained by Hall-effect measurements at room temperature. The preparation of ohmic contacts for Hall-effect measurements is similar to that described in [181]. As shown in figure 11, when the annealing temperatures are lower than  $500^\circ\text{C}$ , it is difficult to obtain reliable Hall data since the films are extremely resistive, especially in the case of  $\text{N}_2$ -ambient annealing. When the annealing temperatures are higher than or equal to  $600^\circ\text{C}$ , the resistivities are around  $2 \Omega \text{ cm}$  and the hole concentrations are around  $3 \times 10^{17} \text{ cm}^{-3}$ . This result may imply that the Mg–H complexes dissociate when the annealing temperatures are higher than or equal to  $600^\circ\text{C}$ . In addition, when the films were

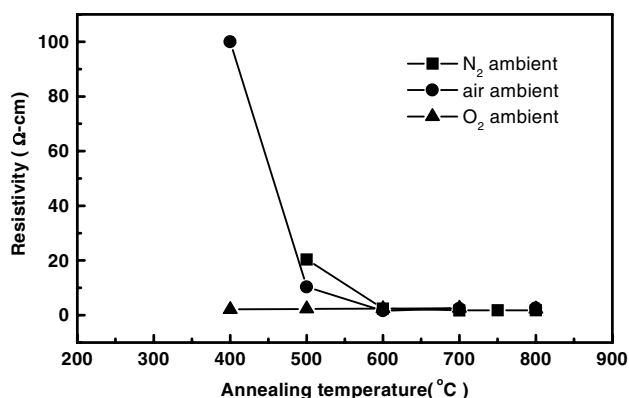


**Figure 11.** The resistivity of p-type GaN films decreasing with increasing annealing temperature, for various ambients [54].

annealed in O<sub>2</sub>-containing environments at below 600 °C, the resistivity was lower than that of films annealed in the N<sub>2</sub> ambient. Surprisingly, low-resistivity p-type GaN can also be obtained by O<sub>2</sub>-ambient annealing at 400 °C, as shown in figure 11. The resistivities and hole concentrations are about 2 Ω cm and  $3 \times 10^{17} \text{ cm}^{-3}$  at room temperature, respectively. This phenomenon could be tentatively interpreted as arising from the low-temperature activation of Mg-doped GaN in O<sub>2</sub>-containing ambient being due to the powerful removal of residual hydrogen from the film. Most reports demonstrated that low-resistivity MOVPE-grown p-type GaN can be achieved by N<sub>2</sub>-ambient annealing above 600 °C. In the light of the reported results of Nakamura *et al* [3, 127], almost no change in resistivity could be observed when the as-grown Mg-doped GaN films were annealed in N<sub>2</sub> ambient with temperatures between room temperature and 400 °C. When the annealing temperatures were larger than or equal to 700 °C, it was demonstrated that the resistivity and hole concentration are about 2 Ω cm and  $3 \times 10^{17} \text{ cm}^{-3}$ , respectively. Considering our results on N<sub>2</sub>-ambient annealed samples, it can be seen that low resistivity can be obtained at annealing temperature of 600 °C. This discrepancy between the results could be attributed to the small amount of residual oxygen in N<sub>2</sub>, since the use of N<sub>2</sub> did not go through an apparatus effecting moisture (H<sub>2</sub>O) and/or O<sub>2</sub> gettering in these annealing experiments. Similar results have also been reported by Hull *et al* [163]. They obtained the hydrogen concentration of Mg-doped GaN annealed in O<sub>2</sub>-gettering N<sub>2</sub> and in 10% O<sub>2</sub>, 90% N<sub>2</sub> ambient. The hydrogen concentration was larger than  $1 \times 10^{19} \text{ cm}^{-3}$  for annealing in O<sub>2</sub>-gettering N<sub>2</sub>, while it decreased to  $4\text{--}5 \times 10^{18} \text{ cm}^{-3}$  for annealing in 10% O<sub>2</sub>, 90% N<sub>2</sub> ambient. One might suggest that the lower resistivity of the p-type GaN annealed in the O-containing ambient is due to enhanced removal of H, which passivates the Mg during MOVPE growth in H-rich ambient. Figure 12 shows the variation of the hole concentration as a function of the temperature. Mg-doped GaN films were annealed in various ambients including O<sub>2</sub>, air, and N<sub>2</sub>. Although the hole concentrations between vary somewhat between these samples, the activation energies ( $\sim 140 \text{ meV}$ ) of Mg in GaN are almost the same, and close to the reported results [157, 159, 160]. Kozodoy *et al* [156] commented that Mg concentration can influence the degree of compensation and the onset of impurity band conduction. The compensation effect appears to drive other effects such as the variation of the ionization energy and hole concentration for Mg-doped GaN. Considering the difference in hole concentration between these annealed samples, as shown in figure 12, one can tentatively suggest that the surface reaction becomes significant during thermal annealing of Mg-doped GaN in O<sub>2</sub>-containing ambients relative to that in pure N<sub>2</sub> ambient. In the case of

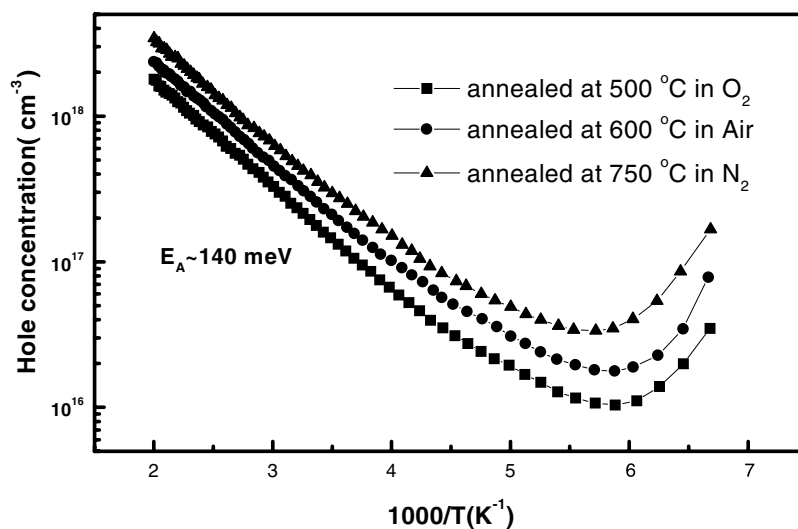


**Figure 12.** The dependence of the hole concentration on the temperature, for samples annealed in oxygen, air, and nitrogen ambients.

$O_2$ -ambient annealing, the maximum hole concentration of  $3 \times 10^{17} \text{ cm}^{-3}$  was obtained at the annealing temperature of  $500 \text{ }^\circ\text{C}$ . The hole concentration decreased to below  $3 \times 10^{17} \text{ cm}^{-3}$  for annealing temperatures above  $500 \text{ }^\circ\text{C}$ , whereas the maximum value was obtained at a temperature of  $600 \text{ }^\circ\text{C}$  in air-ambient annealing. On the other hand, gallium oxide may be generated on the surface and then the oxygen diffuse into the GaN during thermal annealing in  $O$ -containing ambient, especially for those samples annealed over a longer period of time. The incorporation of oxygen into GaN might lead to hole compensation in situations such as that of epitaxial regrowth over  $\text{SiO}_2$  windows or during annealing with  $\text{SiO}_2$  capping layers [167]. It has been reported that the presence of oxygen during the growth process can result in a significant influence on the background n-type conductivity, indicating that  $O$  is a shallow donor [12, 79, 83].

**3.2.2. AlGa<sub>x</sub>N.** As previously discussed, several reports showed that the resistivity of n-type  $\text{Al}_x\text{Ga}_{1-x}\text{N}$  increases with increasing Al content [84–88]. The results of first-principles calculations for native defects in AlN show the similarity to GaN [171–173]. Van de Walle *et al* [169] proposed that the nitrogen vacancy is a high-energy defect in n-type AlN, but it becomes a low-energy defect in p-type AlN. Therefore, for p-type doping, the nitrogen vacancies would be the compensating centres and are more easily formed in AlN than in GaN. In addition, the ionization energy of the acceptor increases with increasing Al content in AlGa<sub>x</sub>N. At present, magnesium is still the only practical p-type dopant for nitride semiconductors. The hole concentration of Mg-doped GaN is still lower than desired due to the high activation energy, particularly for wider-band-gap materials such as high-Al-content nitride alloys. In other words, the medium hole concentration of  $\text{Al}_x\text{Ga}_{1-x}\text{N}$  alloys can be achieved with Mg doping, but decreases rapidly on increasing the Al content. The low doping efficiency is an inherent property of a deep acceptor in wide-band-gap materials. From the calculation of Van de Walle *et al* [74], the ionization energy of Mg acceptor in AlN is about 0.4 eV, which is higher than that in GaN ( $\sim 0.15 \text{ eV}$ ). Temperature-dependent Hall-effect measurements revealed that the activation energy of Mg should be 35 meV lower in  $\text{Al}_x\text{Ga}_{1-x}\text{N}$  ( $x = 0.08$ ) than in

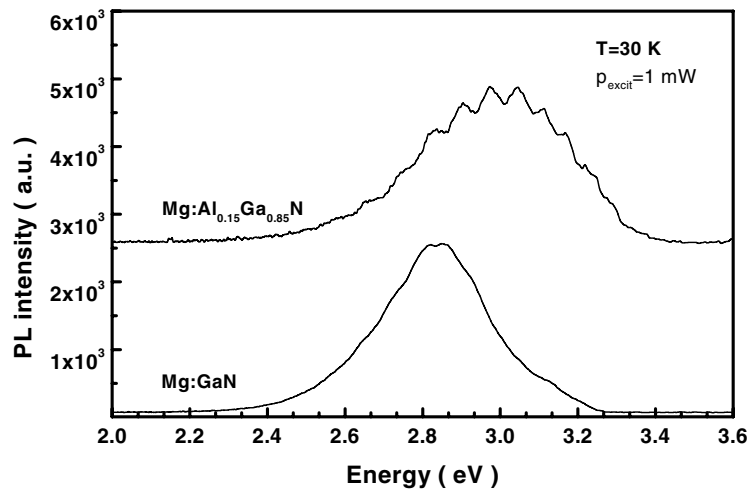
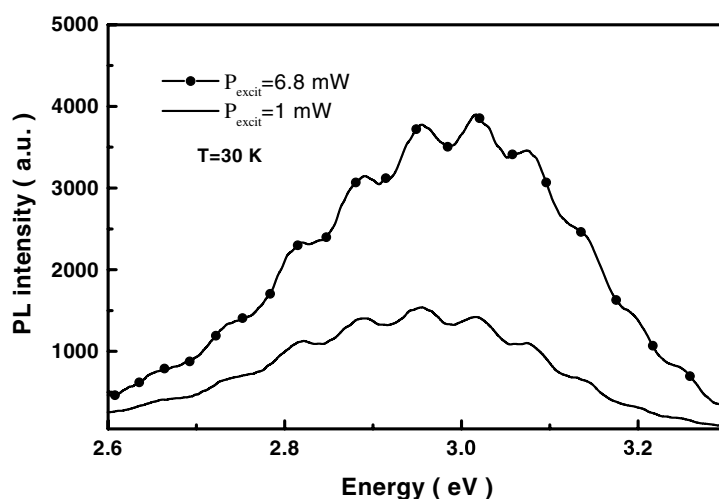


Figure 13. PL spectra of Mg-doped GaN and  $\text{Al}_{0.15}\text{Ga}_{0.85}\text{N}$  taken at 30 K.

GaN [157]. In view of the linearity, this would make the activation energy of the Mg acceptor in AlN 0.44 eV. Suzuki *et al* [175] reported that  $\text{Al}_{0.15}\text{Ga}_{0.85}\text{N}$  has a hole concentration and a thermal activation energy of about  $6.6 \times 10^{16} \text{ cm}^{-3}$  and 250 meV, respectively. They also revealed that the activation efficiency of Mg is about 50% for low-level Mg concentration, and decreases with increasing Mg concentration. Similar results were also observed by Kozodoy *et al* [156]. Suzuki *et al* [175] have tentatively concluded that the reduction of the Mg activation efficiency for high Mg concentration cannot be explained by the effects of background donors and/or residual hydrogen. Still, extra Mg may induce interstitial atoms or other defects such as Mg–Mg pairs, which can therefore diminish the electrical activity. One might suggest that as the Mg concentration is increased beyond a certain value, which depends on the growth conditions, the measured hole concentration would reduce. This might be due to much of the incorporated Mg not being located at the desired substitutional sites, i.e., Ga sites. In addition, the activation energy of Mg in  $\text{Al}_x\text{Ga}_{1-x}\text{N}$  ( $x \geq 0$ ) is strongly influenced by the amount of incorporated Mg, because the high concentration of Mg will form a broad impurity band extending toward the valence band edge, and hence binding energy reduction through a Coulomb interaction between valence band holes and ionized acceptors occurs. Therefore, this suggestion could be adopted to explain the variation in published data for the activation energy of Mg in  $\text{Al}_x\text{Ga}_{1-x}\text{N}$  ( $x \geq 0$ ).

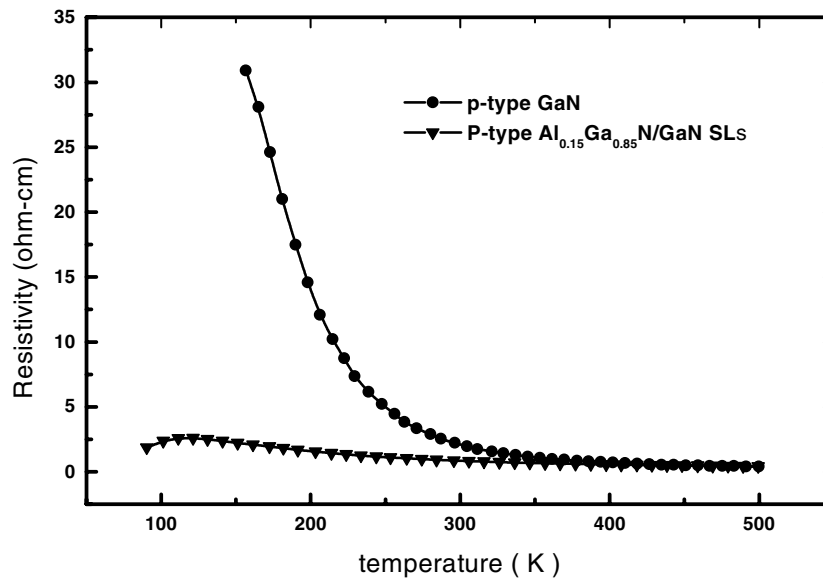
It is well known that the deep-level nature of Mg in GaN limits the possibility of increasing the hole concentration of Mg-doped GaN. This makes it even more difficult to obtain highly conductive p-type  $\text{Al}_x\text{Ga}_{1-x}\text{N}$ . High-quality p-type epitaxial layers are necessary for carrier and optical confinement to fabricate the nitride-based laser diodes. Recent investigations have indicated that the use of Mg-doped  $\text{Al}_x\text{Ga}_{1-x}\text{N}/\text{GaN}$  strained layer superlattices (SLSs) can increase the ionization percentage of the acceptors [4, 5, 230–232]. Optical and electrical properties of SLS structures have been extensively investigated, especially in the AlGaAs/GaAs system [177, 178]. Attempts to further understand  $\text{Al}_x\text{Ga}_{1-x}\text{N}/\text{GaN}$  SLSs have mainly focused on the electrical properties [5, 6].

Figure 13 compares the PL spectra of Mg-doped GaN and  $\text{Al}_{0.15}\text{Ga}_{0.85}\text{N}$  taken at 30 K. According to these data, the PL spectrum of  $\text{Al}_{0.15}\text{Ga}_{0.85}\text{N}$  displays a clear intensity modulation, indicating that the microcavity effect occurs in the layers with a sufficiently small surface



**Figure 14.** PL spectra of Mg-doped  $\text{Al}_{0.15}\text{Ga}_{0.85}\text{N}/\text{GaN}$  SLSs (sample C) at 30 K with different excitation intensities.

roughness. It also shows only one broad band appearing at around 3.0 eV. This spectrum resembles the p-type GaN one in that only one emission peak appears, near 2.85 eV. In addition, this PL peak exhibits a shifting behaviour on varying the He–Cd laser power. This excitation density dependence is attributed to the DAP transition in semiconductors rather than the free-electron–acceptor transition [137]. It is believed that the emission band in Mg-doped  $\text{Al}_{0.15}\text{Ga}_{0.85}\text{N}$  with a peak appearing around 3 eV is attributable to the transitions of the Mg-related shallow level and the deep impurity-related donors [133]. Experimental results indicated that the Mg-related transition in  $\text{Al}_{0.15}\text{Ga}_{0.85}\text{N}$  has an energy about 0.81 eV lower than the transition of undoped  $\text{Al}_{0.15}\text{Ga}_{0.85}\text{N}$ ; the band gap of undoped  $\text{Al}_{0.15}\text{Ga}_{0.85}\text{N}$  is assigned as 3.81 eV. The hole concentration of Mg-doped  $\text{Al}_{0.15}\text{Ga}_{0.85}\text{N}$  is  $\sim 1 \times 10^{17} \text{ cm}^{-3}$  with mobility around  $10 \text{ cm}^2 \text{ V}^{-1} \text{ s}^{-1}$ , as obtained at room temperature from Hall-effect measurements. Table 1 lists the electrical results from Hall-effect measurements. The hole concentration of GaN at room temperature is six times the magnitude of that of the bulk  $\text{Al}_{0.15}\text{Ga}_{0.85}\text{N}$  layer. Although low-resistivity p-type conduction is difficult to achieve in bulk  $\text{Al}_x\text{Ga}_{1-x}\text{N}$  layers, a recent investigation has partially overcome this problem by applying a periodic oscillation of the valence band edge [4–6, 179]. In a typical Mg-doped  $\text{Al}_x\text{Ga}_{1-x}\text{N}/\text{GaN}$  SLS, the strain-induced polarization field can significantly enhance the electrical activity of deep Mg acceptors. Although the free carriers are separated into a parallel sheet in this SLS, the spatial average carrier density is still higher than in a bulk layer. Because of this enhancement of the activation efficiency, the hole concentration of  $\text{Al}_{0.15}\text{Ga}_{0.85}\text{N}/\text{GaN}$  SLS at room temperature can be as high as thirty times that of the bulk  $\text{Al}_{0.15}\text{Ga}_{0.85}\text{N}$  layer [230]. On the other hand, the hole concentration decreases with increase of the flow rate of  $\text{CP}_2\text{Mg}$  for Mg-doped AlGaN [232]. A similar phenomenon was also observed in Mg-doped GaN [56, 175], as shown in figure 6. In summary, the electrical properties observed for Mg-doped  $\text{Al}_{0.15}\text{Ga}_{0.85}\text{N}/\text{GaN}$  superlattices are due to the large strain-induced piezoelectric fields in the superlattices. This large strain-induced piezoelectric field lowers the acceptor level below the Fermi level and transfers the holes into the lowest-energy part of the AlGaN/GaN interfaces. Therefore, high doping efficiency can be achieved by using this heterostructure if the piezoelectric field that is induced is sufficiently large.



**Figure 15.** Resistivities of p-type  $\text{Al}_{0.15}\text{Ga}_{0.85}\text{N}/\text{GaN}$  SLSs and GaN as functions of temperature. Solid triangles represent Mg-doped  $\text{Al}_{0.15}\text{Ga}_{0.85}\text{N}/\text{GaN}$  (16/18 nm) superlattices, and solid circles represent an Mg-doped GaN bulk layer.

**Table 1.** Hall data obtained at room temperature for samples annealed at 750 °C.

Sample	Resistivity ( $\Omega$ cm)	Hole concentration ( $\text{cm}^{-3}$ )	Hall mobility ( $\text{cm}^2 \text{V}^{-1} \text{s}^{-1}$ )
GaN:Mg	1.2	$6 \times 10^{17}$	17
$\text{Al}_{0.15}\text{Ga}_{0.85}\text{N}:\text{Mg}$	4	$1 \times 10^{17}$	10
$\text{Al}_{0.15}\text{Ga}_{0.85}\text{N}/\text{GaN}:\text{Mg}$ SLS	0.75	$3 \times 10^{18}$	5

To explore the origin of the observed emission band, PL measurements were performed at 30 K with two different excitation intensities. Figure 14 shows the PL spectra of Mg-doped  $\text{Al}_{0.15}\text{Ga}_{0.85}\text{N}/\text{GaN}$  SLSs at 30 K with different excitation intensities. The spectra have dominant emission peaks at around 3.0 and 2.95 eV for high-excitation (6.8 mW) and low-excitation (1 mW) conditions, respectively. According to figure 14, the dominant emission band shifts towards a higher energy, around 3.0 eV, on increasing the excitation intensity. This can also be attributed to a DAP transition in semiconductors [137]. In view of the previous discussions, we can infer that the transition of the PL for Mg-doped  $\text{Al}_{0.15}\text{Ga}_{0.85}\text{N}/\text{GaN}$  superlattices is due to a Mg-related DAP transition.

Figure 15 shows the resistivities of the p-type  $\text{Al}_{0.15}\text{Ga}_{0.85}\text{N}/\text{GaN}$  SLS (16/8 nm) and GaN as functions of temperature. The resistivities of SLSs are far smaller than those of GaN bulk layers within low-temperature regions. The resistivity of Mg-doped GaN increases rapidly with decrease of the temperature. For Mg-doped GaN, the free carriers mainly result from thermal ionization; therefore, the resistivity of Mg-doped GaN exhibits a strong temperature dependence. For p-type  $\text{Al}_{0.15}\text{Ga}_{0.85}\text{N}/\text{GaN}$  SLSs, the resistivity increases slowly with decreasing temperature. This phenomenon can be explained by the free carriers in this SLS resulting mainly from band bending caused by the piezoelectric fields. Thus, the p-type conductivity of this structure exhibits a weaker temperature dependence. Owing to

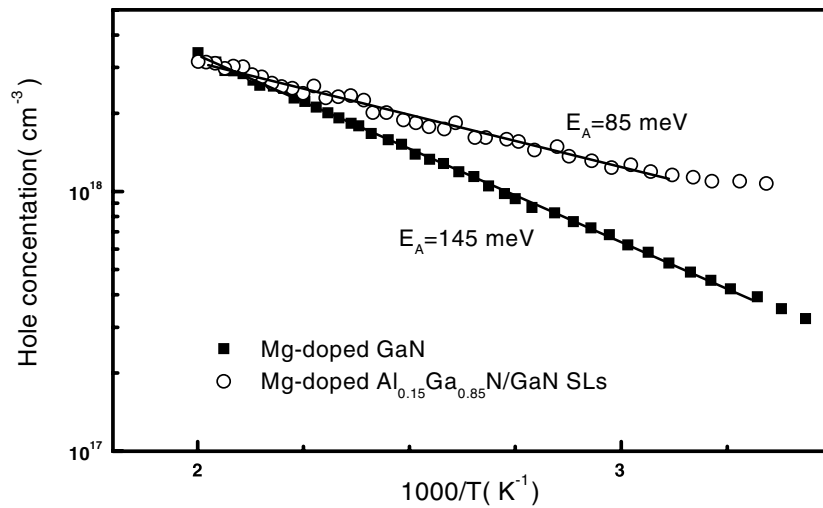


**Figure 16.** The hole concentration versus the reciprocal temperature. Open circles represent Mg-doped 25-period  $\text{Al}_{0.15}\text{Ga}_{0.85}\text{N}/\text{GaN}$  (10/10 nm) superlattices, and solid squares represent an Mg-doped GaN bulk layer.

the higher activation efficiency of Mg in the  $\text{Al}_x\text{Ga}_{1-x}\text{N}/\text{GaN}$  SLS, high-hole-concentration ( $>10^{18} \text{ cm}^{-3}$ ) p-type nitride semiconductors can easily be achieved [5, 6, 180]. Figure 16 shows the hole concentration versus the reciprocal temperature for an Mg-doped 25-period  $\text{Al}_{0.15}\text{Ga}_{0.85}\text{N}/\text{GaN}$  SLS. At room temperature, the hole concentration is  $1 \times 10^{18} \text{ cm}^{-3}$ . The data for Mg-doped GaN with a hole concentration of  $4 \times 10^{17} \text{ cm}^{-3}$  are also depicted. The 25-period  $\text{Al}_{0.15}\text{Ga}_{0.85}\text{N}/\text{GaN}$  (10/10 nm) SLS exhibits a linear dependence versus  $1/T$  for temperature over the range of 300–500 K. The measured activation energy for the  $\text{Al}_{0.15}\text{Ga}_{0.85}\text{N}/\text{GaN}$  SLSs is 85 meV, which is significantly lower than for the GaN bulk layer ( $\sim 140$  meV). This is consistent with previously reported data [4–6]. It may indicate that Mg-doped  $\text{Al}_x\text{Ga}_{1-x}\text{N}/\text{GaN}$  SLSs would be useful in devices requiring transport of holes only—especially in certain optoelectronic devices.

The specific contact resistance of metal on a p-type  $\text{Al}_x\text{Ga}_{1-x}\text{N}/\text{GaN}$  SLS is expected to be smaller than those of metal contacts, such as Ni/Au [181, 182] or Pt/Ni/Au [183, 184] on p-type GaN. The specific contact resistance ( $\rho_c$ ) of Ni/Au (6/14 nm) on an Mg-doped  $\text{Al}_{0.15}\text{Ga}_{0.85}\text{N}/\text{GaN}$  SLS is around  $4 \times 10^{-6} \Omega \text{ cm}^2$  after annealing in an  $\text{N}_2$  ambient at a temperature of  $650^\circ\text{C}$ , as shown in figure 17. This  $\rho_c$ -value is much smaller than that of the typical Ni/Au contact to Mg-doped GaN ( $4 \times 10^{-6}$ – $1 \times 10^{-2} \Omega \text{ cm}^2$  [181–184, 231]). Generally, for metal contacts on semiconductors with high hole concentrations, the thermionic field emission or the tunnelling effect of the carrier transport will dominate the conduction mechanism. On the other hand, one can expect p-type nitride semiconductors with high hole concentrations ( $>10^{18} \text{ cm}^{-3}$ ), such as Mg-doped  $\text{Al}_x\text{Ga}_{1-x}\text{N}/\text{GaN}$  SLSs, to enhance the tunnelling effect of free carriers and thereby reduce the contact resistance of the metal–semiconductor interface. In addition, the effect of the strain-induced polarization field in the SLS is enhanced by the depletion field and thus reduces the tunnelling distance and the contact resistance [185].

**3.2.3. InGaN.**  $\text{In}_x\text{Ga}_{1-x}\text{N}$  is mostly used as an active layer, which is unintentionally doped or intentionally doped with silicon [102–106]. Generally, in nitride-based optical devices, p-type

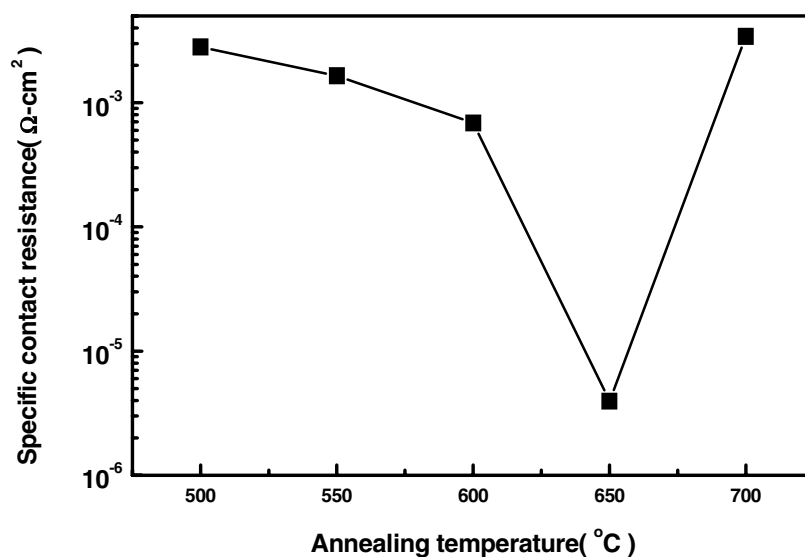


**Figure 17.** The specific contact resistivity of Ni/Au on Mg-doped  $\text{Al}_{0.15}\text{Ga}_{0.85}\text{N}/\text{GaN}$  SLSs versus annealing temperature (exposure for 5 min).

GaN is the most common contact layer for p-type electrodes. Clearly, p-type  $\text{In}_x\text{Ga}_{1-x}\text{N}$  appears promising for use as a p-type contact layer with low contact resistance, since the band gap of  $\text{In}_x\text{Ga}_{1-x}\text{N}$  is smaller than that of GaN. In addition, it was expected that the p-type  $\text{In}_x\text{Ga}_{1-x}\text{N}$  active layer would enhance the hole injection efficiency as compared with intrinsic- or n-type  $\text{In}_x\text{Ga}_{1-x}\text{N}$  active layers in LED structures [186]. For electrical devices, p-type  $\text{In}_x\text{Ga}_{1-x}\text{N}$  is also a potential base layer for heterojunction bipolar transistors (HBT), since with the larger band-gap difference between emitter and base, the higher doping level would lead to significant improvement of the device performance. Up to now, only a few papers have given electrical properties of  $\text{In}_x\text{Ga}_{1-x}\text{N}$  materials [187, 188]. Most reports were focused on the optical properties of  $\text{In}_x\text{Ga}_{1-x}\text{N}$  layers and their heterostructures [66–69, 97–110, 189]. Mg-doped p-type  $\text{In}_{0.09}\text{Ga}_{0.91}\text{N}$  film was first demonstrated in 1995, by Yamasaki *et al* [184]; after rapid thermal annealing in nitrogen ambient at atmospheric pressure, a hole concentration at room temperature of  $\sim 7 \times 10^{17} \text{ cm}^{-3}$  was achieved. This report also suggested that the activation energy of Mg in  $\text{In}_{0.09}\text{Ga}_{0.91}\text{N}$  is around 204 meV and that the peak wavelength of the PL spectra varied from 470 to 490 nm. It is well known that the emission peak position of Mg-doped GaN can vary from 430 to 450 nm [190]. Just like Mg-doped GaN, as-grown Mg-doped  $\text{In}_x\text{Ga}_{1-x}\text{N}$  shows high resistivity but become p-type conductive upon thermal annealing. Figure 18 shows the hole concentration of Mg-doped  $\text{In}_x\text{Ga}_{1-x}\text{N}$  at room temperature determined by Hall-effect measurements. These Mg-doped  $\text{In}_x\text{Ga}_{1-x}\text{N}$  epitaxial layers were grown by MOVPE at a temperature of 780 °C. The post-growth annealing was performed in  $\text{N}_2$  ambient at 700 °C for 25 min. The hole concentrations of Mg-doped  $\text{In}_{0.04}\text{Ga}_{0.96}\text{N}$  and  $\text{In}_{0.23}\text{Ga}_{0.77}\text{N}$  are  $\sim 8 \times 10^{17}$  and  $\sim 1 \times 10^{19} \text{ cm}^{-3}$ , respectively. For comparison, Mg-doped GaN was also grown, using  $\text{N}_2$  as the carrier gas, with the same  $\text{CP}_2\text{Mg}$  flow rate [236]. The hole concentration of Mg-doped GaN is  $\sim 3 \times 10^{17} \text{ cm}^{-3}$ . As shown in figure 18, the hole concentrations reported by Kumakura *et al* [191] are larger than our data when the In content ranges from 4 to 14%. This may be attributed to the variations of n-type background carrier concentrations and the resulting different compensation ratios.

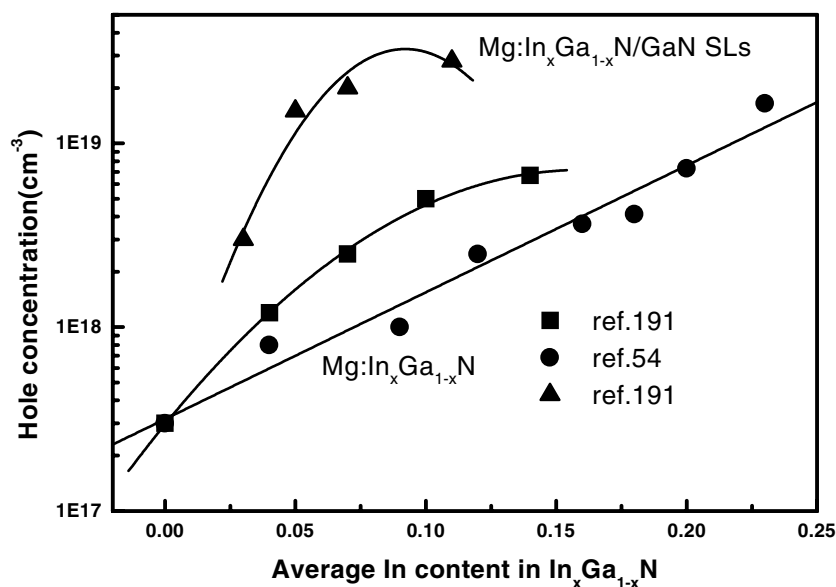


**Figure 18.** Hole concentrations of Mg-doped  $\text{In}_x\text{Ga}_{1-x}\text{N}$  and  $\text{In}_x\text{Ga}_{1-x}\text{N}/\text{GaN}$  SLSs at room temperature as functions of average In content.

In addition, the PL spectrum of  $\text{In}_{0.1}\text{Ga}_{0.9}\text{N}$  with a peak wavelength of around 450 nm was significantly enhanced by thermal annealing, as shown in figure 19. For p-type  $\text{In}_x\text{Ga}_{1-x}\text{N}$  films, the peak position of the PL spectrum is expected to shift toward longer wavelengths with increasing In content. As shown in figure 19, the peak position of p-type  $\text{In}_x\text{Ga}_{1-x}\text{N}$  varied from 450 to 520 nm as the In mole fraction increased from 10 to 23%. A comparison of the PL peak intensity, for both the as-grown and annealed samples, as shown in figure 19, shows that the peak intensity increases by eight orders of magnitude upon 700 °C annealing. Similar results had also been observed for Mg-doped GaN [3, 121, 127, 234]. However, the peak intensity of the annealed sample was weaker than that for the as-grown sample, especially for high-In-content samples. This reduced intensity might be due to the excessive surface dissociation occurring during the annealing process. As the growth temperatures of Mg-doped  $\text{In}_x\text{Ga}_{1-x}\text{N}$  films were changed from 700 to 800 °C, the In content of the Mg-doped  $\text{In}_x\text{Ga}_{1-x}\text{N}$  shifted from  $x = 0.3$  to 0.04. Notably, the  $\text{In}_{0.1}\text{Ga}_{0.9}\text{N}$  growth temperature (780 °C) was higher than the annealing temperature (750 °C). Thus, this sample did not significantly degrade during thermal annealing. However, the  $\text{In}_{0.23}\text{Ga}_{0.77}\text{N}$  growth temperature was 720 °C, which was close to the annealing temperature. Therefore, optical degradation might occur during the annealing process for high-In-content  $\text{In}_x\text{Ga}_{1-x}\text{N}$  samples.

Recently, Kumakura *et al* [191] demonstrated that Mg-doped  $\text{In}_{0.14}\text{Ga}_{0.86}\text{N}$  with hole concentrations at room temperature as high as  $6.7 \times 10^{18} \text{ cm}^{-3}$  can be achieved. The activation energy of Mg in  $\text{In}_x\text{Ga}_{1-x}\text{N}$  decreases with increase of the In content. In group III nitride semiconductors, it has been shown that the activation energy of Mg in AlGaIn increases with increasing band-gap energy [157, 175, 192], as shown in figure 20. Kumakura *et al* reported that the activation energy of Mg in  $\text{In}_{0.1}\text{Ga}_{0.9}\text{N}$  is around 98 meV. This value is dramatically smaller than that derived from the data of Yamasaki *et al* [186]; this might be due to the lower n-type background concentration of InGaIn. Kumakura *et al* [193] also showed that Mg-doped  $\text{In}_x\text{Ga}_{1-x}\text{N}$  GaN SLSs with hole concentrations at room temperature as high as  $2.8 \times 10^{19} \text{ cm}^{-3}$

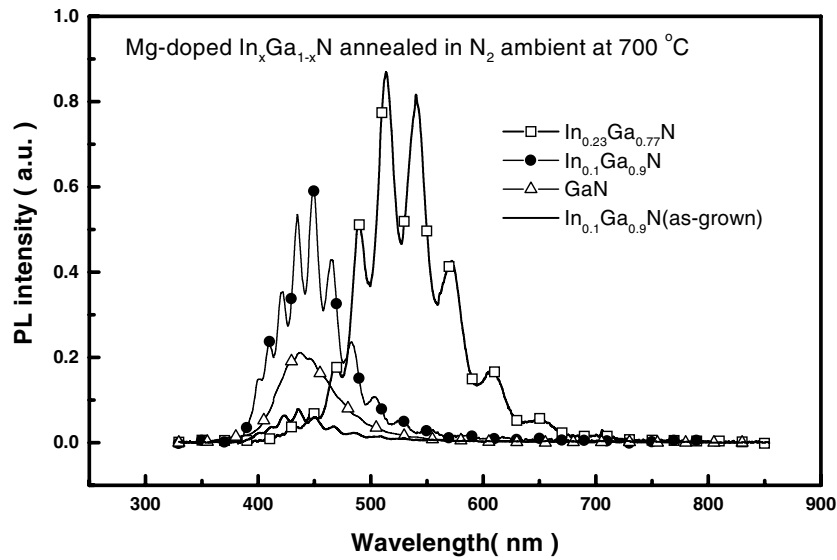


Figure 19. Room temperature PL spectra of Mg-doped  $\text{In}_x\text{Ga}_{1-x}\text{N}$ .

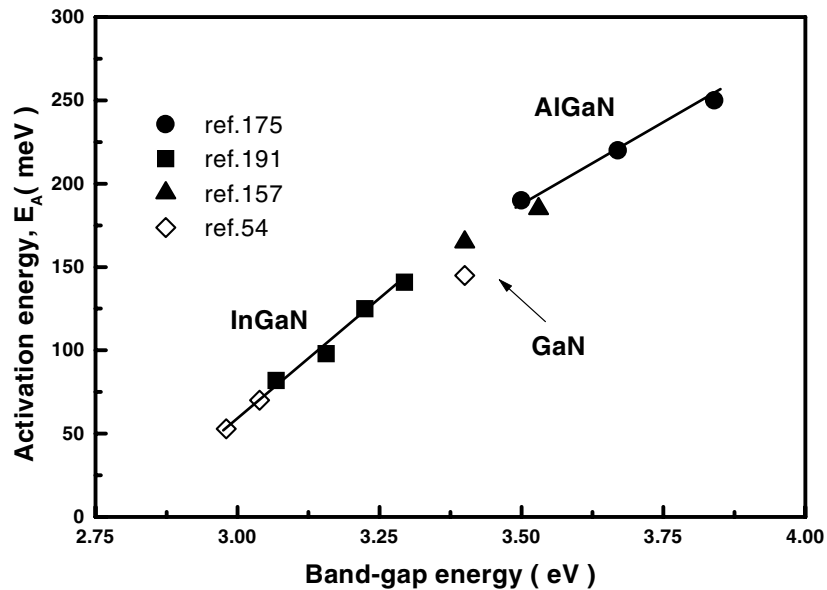
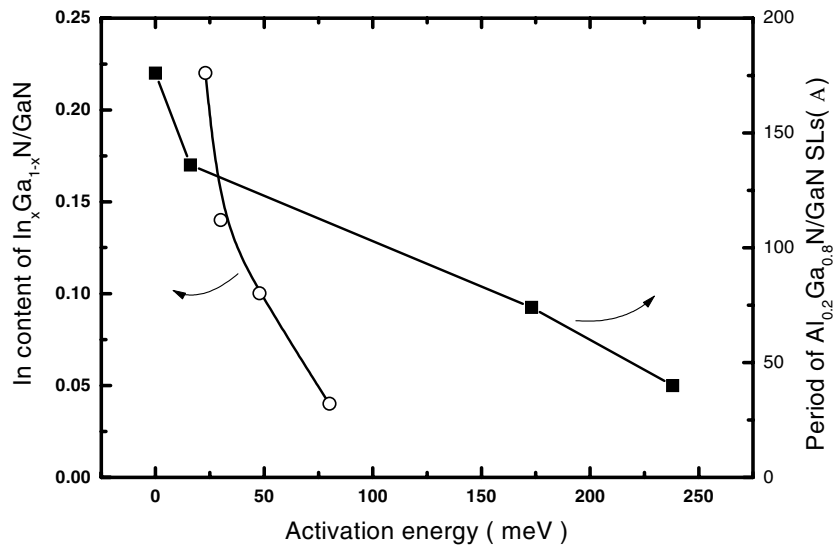


Figure 20. Activation energies of Mg in p-type  $\text{Al}_x\text{Ga}_{1-x}\text{N}$ , GaN, and  $\text{In}_x\text{Ga}_{1-x}\text{N}$  as functions of the band-gap energy [54, 157, 175, 191].

( $x = 0.22$ ) can be obtained. Two possible causes of the high hole concentration were proposed by Kumakura *et al.* The general viewpoint is that the piezoelectric field is considered to dominate the modulation of the band structures for the  $\text{In}_x\text{Ga}_{1-x}\text{N}/\text{GaN}$  SLSs because of the large lattice mismatch between  $\text{In}_x\text{Ga}_{1-x}\text{N}$  and GaN. Thus, significant band bending takes place in  $\text{In}_x\text{Ga}_{1-x}\text{N}/\text{GaN}$  SLS (similarly to in the  $\text{Al}_x\text{Ga}_{1-x}\text{N}/\text{GaN}$  SLSs), and results in a more efficient activation of dopants. Manz *et al* [194] reported that the value of  $\Delta E_V$  (the energy



**Figure 21.** Activation energies of Mg acceptors in p-type  $\text{Al}_{0.2}\text{Ga}_{0.8}\text{N}/\text{GaN}$  and  $\text{In}_x\text{Ga}_{1-x}\text{N}/\text{GaN}$  as functions of the period of the SLS and the In content. Open circles indicate data from [191], and solid squares indicate data from [5].

difference between GaN and strained  $\text{In}_{0.14}\text{Ga}_{0.86}\text{N}$ ) is comparable to that for the Mg acceptor levels in GaN. If the  $\Delta E_V$  value is larger than the energy difference between the Mg acceptor levels in GaN, the holes in the GaN barrier layers can easily be released to the  $\text{In}_x\text{Ga}_{1-x}\text{N}$  well layers, the result being high spatially averaged hole concentrations even at low temperature. The activation energy of Mg acceptors in Mg-doped  $\text{In}_x\text{Ga}_{1-x}\text{N}/\text{GaN}$  SLSs decreases with increasing InN content. Figure 21 shows the activation energies of Mg acceptors in p-type  $\text{Al}_{0.2}\text{Ga}_{0.8}\text{N}/\text{GaN}$  and  $\text{In}_x\text{Ga}_{1-x}\text{N}/\text{GaN}$  as functions of the period of the SLS and the indium content, respectively. Because of the strain in these structures, the total thickness in a period is limited by the critical thickness. In a fixed period, the strain between the barrier and well layers is proportion to the Al (or In) content in the  $\text{In}_x\text{Ga}_{1-x}\text{N}/\text{GaN}$  ( $\text{Al}_x\text{Ga}_{1-x}\text{N}/\text{GaN}$ ) SLS. It is well known that the critical thickness decreases with increase of the mismatch (strain) between  $\text{In}_x\text{Ga}_{1-x}\text{N}$  (or  $\text{Al}_x\text{Ga}_{1-x}\text{N}$ ) and GaN, i.e., increase of the In or Al content. On the other hand, the high hole concentration in the SLS is attributed to the strain-induced piezoelectric field dramatically increasing the activation efficiency (reducing the activation energy) of the Mg acceptors in the SLS, as mentioned above for the Mg-doped  $\text{Al}_x\text{Ga}_{1-x}\text{N}/\text{GaN}$  SLS. The piezoelectric field is related to the critical thickness, i.e. the strain tensor component which is determined by the difference between the lattice constant for  $\text{In}_x\text{Ga}_{1-x}\text{N}$  ( $\text{Al}_x\text{Ga}_{1-x}\text{N}$ ) and that for GaN.

#### 4. Doping by diffusion and ion implantation

In general, two standard techniques are employed in the doping of semiconductors. The first is the solid-state diffusion technique, whereby impurity atoms are introduced into the surface regions of a semiconductor and caused to diffuse into the material by heating the semiconductor to high temperatures. In the second technique, ion implantation, dopant ions are accelerated to energies of hundreds of kiloelectron volts and fired at the semiconductors where they become implanted impurities. The techniques of diffusion and ion implantation are attractive for the

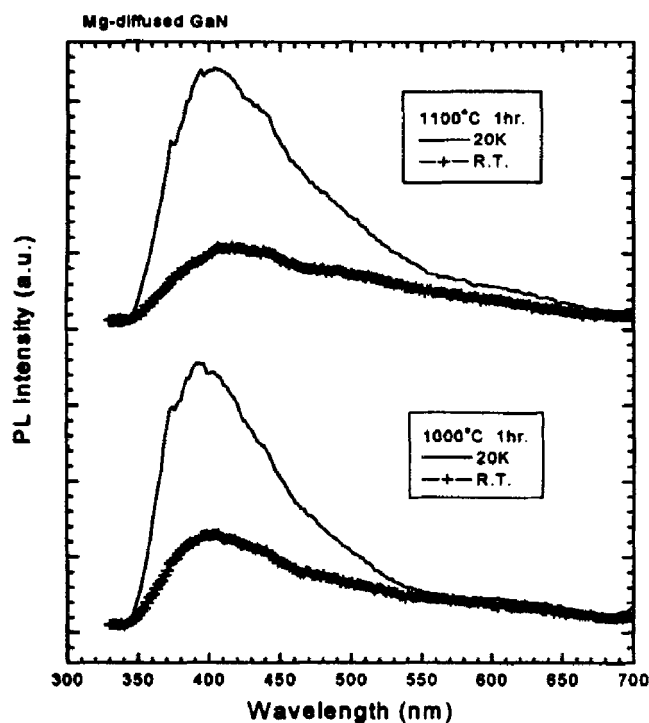


Figure 22. PL spectra of Mg-diffused GaN taken at room temperature and 20 K.

fabrication of devices related to III–V compounds and GaN because they can introduce well-defined impurity concentrations in selected regions.

#### 4.1. Diffusion process

Doping by diffusion is a conventional processing technique. For GaN, there has been little diffusion work reported. In 1994, Rubin *et al* reported that p-type GaN can be obtained by Mg diffusion with a hole concentration of  $2 \times 10^{16} \text{ cm}^{-3}$  [195]. A very critical temperature-dependent effect on the diffusion process was also mentioned. Recently, Yang *et al* [196] reported that the diffused and annealed samples consistently show p-type conductivity with average hole concentrations in the range of  $10^{16}$ – $10^{17} \text{ cm}^{-3}$ . In addition, the samples showed an emission band with a peak at 3.27 eV followed by two longitudinal optical (LO) phonon replicas with a separation of  $\sim 90 \text{ meV}$  at 10 K. Figure 22 shows the room temperature and 20 K PL spectra of the Mg-diffused GaN [197]. These PL spectra show only one broad violet emission at about 400 nm. It can be attributed to an Mg-related emission which is similar to that exhibited by MOCVD-grown Mg-doped GaN. Figure 23 shows the SIMS depth profiles and the resulting fits for Mg-diffused GaN samples which were diffused at 1000 and 1100 °C in a sealed quartz ampoule for 1 h [197]. The concentration of foreign atoms due to diffusion in a solid is known as the error function. According to the fitting of this error function, the activation energy of the Mg dopants for diffusion in GaN is 1.3 eV. When the diffusion temperature is  $\leq 900 \text{ °C}$ , blue emission cannot be detected in Mg-diffused GaN, as shown in figure 24 [198]. In other words, the PL spectrum of the 900 °C diffused samples consists of a near-band-edge emission, a yellow luminescence, and a donor–acceptor (DA)

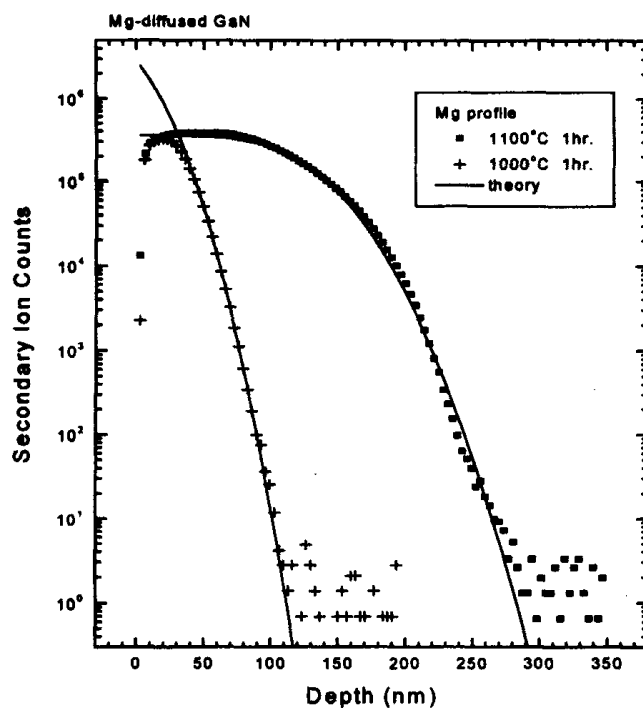


Figure 23. SIMS depth profiles and the resulting fits for Mg-diffused GaN samples which were diffused at 1000 and 1100 °C in a sealed quartz ampoule for 1 h.

emission with LO phonon replicas; it resembles a typical PL spectrum of as-grown undoped GaN [198–202]. This phenomenon could suggest that Mg diffused into the GaN as a very thin layer when the temperature was  $\leq 900$  °C. In 1999, Pearton *et al* [203] indicated that oxygen diffusion into SiO<sub>2</sub>-capped GaN was clearly observed after 900 °C annealing. They suggested that the high density of dislocations in the GaN strongly affects the effective penetration depth. It is thought that surface dissociation becomes significant during high-temperature annealing for GaN, especially in O<sub>2</sub>-containing ambients. In addition, oxygen incorporation into GaN might cause autodoping in situations such as during thermal annealing with an SiO<sub>2</sub> cap layer or epitaxial overgrowth over an SiO<sub>2</sub> window. It is possible that oxygen diffused in and/or Si might substitute for nitrogen and/or gallium, respectively, and thereby cause conduction-type conversion.

For n-type GaN, a heavily doped surface layer formed by a Si diffusion process has been induced to improve the ohmic contact [204]. The preparation of diffusion samples was initiated by the deposition of Si films on the GaN epitaxial layers and this was followed by the deposition of SiO<sub>2</sub> capping layers. The SiO<sub>2</sub> layer was used to prevent the Si from evaporating from the GaN surface during the thermal annealing in the nitrogen ambient for 2 h. To prove that the Si diffusion process causes improvement of the ohmic contact to the n-type GaN, Ni/Al/Ti (300/1200/150 Å) metal contacts were deposited on Si-diffused GaN and this was followed by 800 °C RTA treatment for 30 s. Lin *et al* demonstrated that the specific contact resistivities clearly decreased from  $3 \times 10^{-5}$  to  $6 \times 10^{-7}$   $\Omega$  cm<sup>2</sup> as the Si diffusion temperature increased from 825 to 1000 °C. These results suggested that the improved ohmic characteristic was caused by n<sup>+</sup>-type GaN formed by the Si diffusion process.

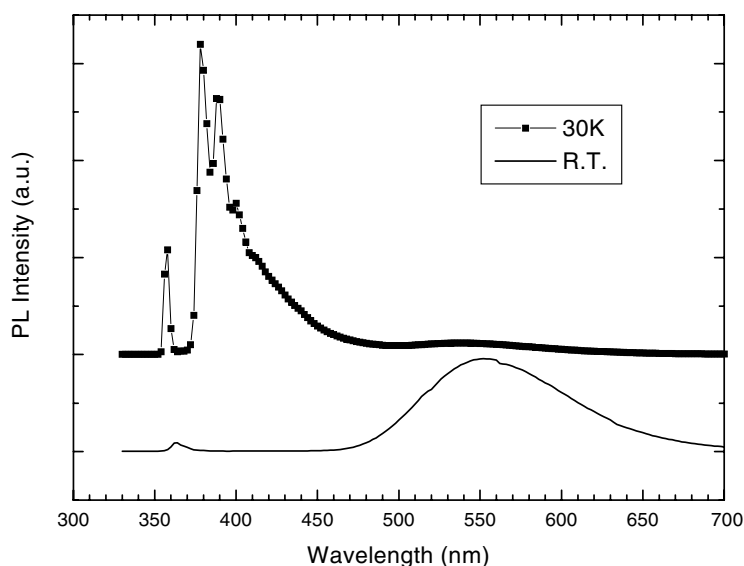


Figure 24. PL spectra of Mg-diffused GaN with diffusion temperatures  $\leq 900^\circ\text{C}$ .

#### 4.2. Doping by ion implantation

Ion implantation is one of the most commonly used processes in semiconductor technology. It is particularly useful for achieving a laterally varied doping and isolation profile across a semiconductor wafer. Forming a p–n junction by ion implantation is one of the key processes in the fabrication of a MOSFET. In the past few years, the achievement of p-type and controlled n-type doping during epitaxial growth in III–V compounds has seen extensive application in production of GaN-based photonic devices as well as high-temperature/high-power electronic devices [1]. However, the use of ion implantation for doping in GaN device technology is still not well developed. In 1969, Masuka and Tietjen showed that the implanted impurities, such as Mg and Zn, in GaN can behave as emission centres. In the early 1970s, Pankove and Hutchby [13, 14] performed work on implantation in GaN. They reported primarily on the optical properties of GaN implanted with a host of elements. The PL characteristics of Zn-implanted GaN, annealed under high pressure and high temperature, have also been reported by Suski *et al* [205]. In addition to the high temperatures and high pressures, high dislocation densities causing a significant diffusion of implanted Zn atoms in GaN films were also commented on by Suski *et al*. According to the calculated results [206], beryllium (Be) is a more promising candidate for the p-type doping of GaN. To date, Be-doped GaN films have only been grown by MBE, since Be precursors suitable for use in MOVPE are not available [207–209]. p-type conduction of Be-doped GaN, which was determined by hot-probe measurement, with an ionization energy of 0.25 eV deduced from PL spectra, was reported by Salvador *et al* [208]. p-type conductivities as high as  $50\text{ V cm}^{-1}$  can also be achieved in cubic Be-doped GaN by reactive codoping, which uses Be as the acceptor species and O as the reactive donor to convert isolated Coulomb scatterers into dipole scatterers [207]. In addition, the incorporation of Be into GaN films by ion implantation has also been performed [210–212]. Ronning *et al* reported that isolated Be has a ionization energy of  $150 \pm 10\text{ meV}$  and that a PL peak at 3.45 eV can be assigned to a band–acceptor transition. This ionization energy of Be in GaN was determined from the PL spectra which were nearly identical to those of Mg-doped

GaN grown by MOVPE. However, the electrical properties of Be-implanted GaN have not appeared in the literature. In the first half of the 1990s, research on ion implantation into GaN was mostly aimed at the realization of p-type materials. However, only a few successes in realizing p-type GaN have been achieved by ion implantation [15, 16, 195]. Rubin *et al* [195] developed p-type GaN by means of low-energy (40–60 keV) Mg-ion implantation in 1994, but were not able to achieve p-type conduction at higher implantation energies. They commented that films implanted with Mg atoms at lower energies can recover to their original lattice parameter after annealing at 800 °C, in contrast to the case for high-energy Mg-implanted samples. Pearton *et al* [15] has also used Mg as a p-type dopant, with co-implantation of P, to produce a p-type region, but Mg<sup>+</sup> or P<sup>+</sup> implantation alone did not produce detectable doping effects. The purpose of the Mg<sup>+</sup>/P<sup>+</sup> co-implantation was to increase the vacancy concentration and promote the ‘substitutionality’ of the Mg upon thermal annealing. Subsequently, p-type conduction was achieved by Ca implantation alone or Ca<sup>+</sup>/P<sup>+</sup> co-implantation in GaN after thermal annealing at 1100 °C or higher [16]. A very high activation efficiency of around 100% and a low ionization energy of 169 meV were obtained. This result is close to Strite’s theoretical hypothesis, according to which Ca should be a shallower acceptor in GaN than Mg; this assertion is based on d-state-electron relaxation effects in GaN and the lack of d-state electrons in Ca [213]. The ionization energy of 169 meV for samples implanted with only Ca<sup>+</sup> or co-implanted with Ca<sup>+</sup>/P<sup>+</sup> is very close to that for Mg<sup>+</sup>/P<sup>+</sup> co-implanted GaN films [214] and is slightly higher than those for epitaxial Mg-doped GaN [98, 159–161]. Additionally, Zolper *et al* reported that the activation efficiency is close to 100% for Ca<sup>+</sup> implanted in GaN, on the basis of an ionization energy of 169 meV. Although Ca<sup>+</sup> seems a good candidate for use as a p-type dopant in GaN, epitaxial Ca-doped p-type GaN has not been achieved yet.

Considering the crystalline quality of implanted GaN, implanted GaN could be amorphous before annealing. Generally, high doses of ions are used for implantation into the GaN due to the low activation efficiency. Consequently, the processes of scattering of impurity ions in crystal cause severe structural damage, which results in a small amount of electrical activity of implanted impurities, and a subsequent high-temperature annealing process is necessary to recover the crystalline structure. In figure 25, no significant diffraction peaks for as-implanted GaN samples, implanted with Mg and Be, was detected, since the structure of the as-implanted GaN is severely damaged. After the annealing at 1000 °C, a distinct diffraction peak can be detected for the annealed Mg- and Be-implanted GaN samples. But the spectra are much wider than those of undoped samples. Similar results were also observed for the diffraction peaks of [10 $\bar{1}$ 1] and [10 $\bar{1}$ 3]. These results indicate that the RTA treatment only produces partial recovery of the damaged GaN crystal structure. Note that the in-plane x-ray diffraction measurement is sensitive to the near-surface region only. Turning to the [0002] direction, the x-ray diffraction spectra for as-implanted, annealed, and undoped GaN samples are also shown in figure 26 [224]. There are two distinct peaks in the GaN [0002] direction for the as-implanted GaN films, implanted with Mg<sup>+</sup> (150 keV/5 × 10<sup>13</sup> cm<sup>-2</sup>) and Be<sup>+</sup> (200 keV/5 × 10<sup>14</sup> cm<sup>-2</sup>). The spectra of the as-implanted samples show a two-layer structure. Peak A might be attributed to the larger lattice parameter in the *c*-axis direction resulting from the implanted region of GaN with the thickness of ~0.5 μm. Peak B might be due to an as-grown GaN layer (undoped) below the implanted region. The lattice constant was dilated in the *c*-axis direction upon implantation. Similar phenomena were also observed by Liu *et al* for Ca<sup>+</sup> implantation at 77 K [215]. The momentum (*Q*) difference between these two peaks is 0.006 Å<sup>-1</sup> [216] for Mg-ion-implanted GaN, as shown by curve (b) in figure 26. The estimated FWHMs for peak A and peak B are 0.046 and 0.037 Å<sup>-1</sup>, respectively [216]. There is only one diffraction peak observed after the 1000 °C RTA, shown in curve (c) in figure 26. The FWHM is 0.005 Å<sup>-1</sup>, which is nearly twice that for the undoped GaN sample (FWHM: 0.002 Å<sup>-1</sup>) [216]. It is suggested

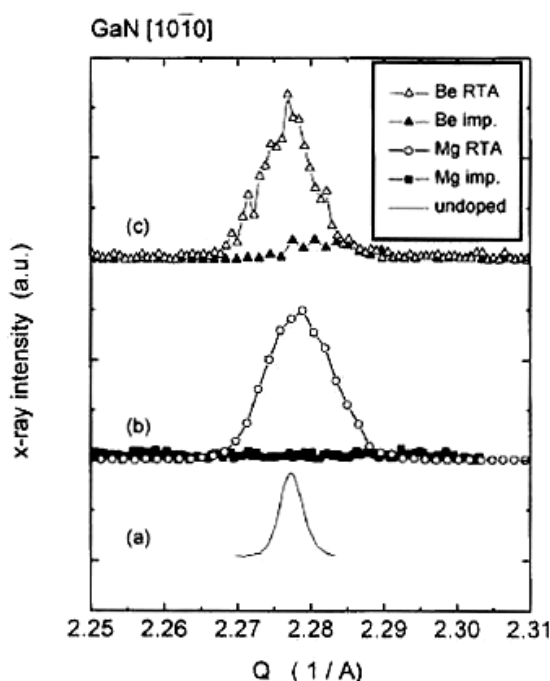


**Figure 25.** X-ray diffraction spectra for as-implanted GaN, implanted with Mg and Be, taken in the in-plane  $[10\bar{1}0]$  direction.

that the RTA-treated Mg-ion-implanted sample still shows microstrain along the  $c$ -axis. This result indicates that RTA treatment had only effected partially recovery of the damaged GaN lattice structure. The corresponding coherent lengths are greater than 1150 and 2300 Å for the RTA-treated Mg-implanted GaN and the undoped GaN samples, respectively [217]. This means that the undoped GaN has a lattice structure with longer-range ordering. There are two distinct peaks separated by  $0.008 \text{ \AA}^{-1}$  [216] in curve (d) of figure 26 for Be-implanted GaN; this separation is larger than that for Mg-implanted GaN. The larger peak separation in the beryllium-ion-implanted sample might be due to the higher dose inducing a larger strain strength along the GaN  $c$ -axis. We also observe two distinct peaks along the GaN  $[0004]$  direction, with nearly twice the separation found along the GaN  $[0002]$  direction, for both Be- and Mg-implanted GaN samples. This result clearly indicates that the peak shift is due to a strain effect. Similar phenomena were observed in the case of ion-implanted GaAs as well [218]. Table 2 lists the lattice constant ratios  $d_1/d_0$  for Be- and Mg-implanted GaN, where  $d_1$  and  $d_0$  are the lattice constants for the implanted region and the undoped region of the GaN, respectively. It can be seen that the implanted region has a larger lattice constant than the as-grown undoped region. The lattice constant changes along the  $c$ -axis for the Be- and Mg-implanted GaN are 0.3 and 0.25%, respectively. Although the atom size of Be is smaller than that of Mg, beryllium implantation, in which the dose is ten times higher than that for Mg implantation, induced a nearly 0.05% greater change,  $\Delta d_1/d_0$ , than Mg implantation for GaN in the  $c$ -axis direction. Therefore, the implantation dose plays an important role in structural damage as well. The dose dependence of damage formation in Si-implanted GaN has also been reported by Tan *et al* [219]. For Ca-implanted GaN with a dose of  $3 \times 10^{14} \text{ cm}^{-2}$ ,  $d_1/d_0$  in the  $[0002]$  direction is larger than for Be-implanted GaN [215].  $\Delta d_1/d_0$  for calcium-implanted

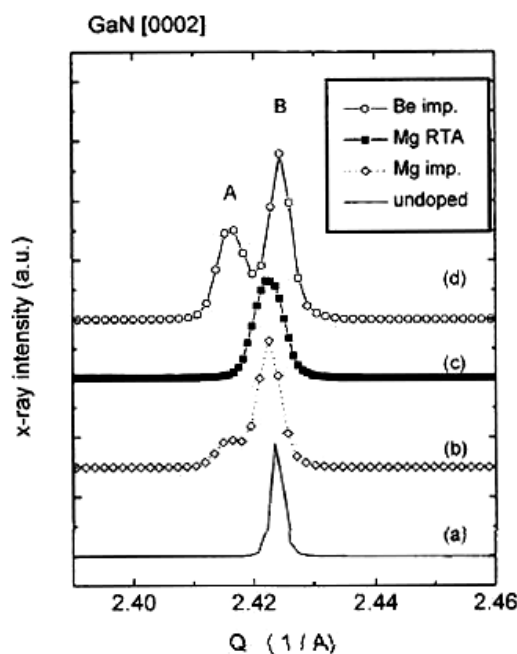


**Figure 26.** X-ray diffraction spectra for (d), (b) as-implanted, (c) annealed, and (a) undoped GaN taken in the [0002] direction.

**Table 2.** The lattice constant ratio  $d_1/d_0$  for Be- and Mg-implanted GaN, where  $d_1$  and  $d_0$  are the lattice constants for the implanted region and the undoped region of the GaN, respectively.

Lattice	Be implantation	Mg implantation
[0002]	$1.0031 \pm 0.0005$	$1.0025 \pm 0.0005$
[10 $\bar{1}$ 3]	$1.0017 \pm 0.0005$	$1.0017 \pm 0.0005$

GaN was greater than that for beryllium-implanted GaN due to the atom size of calcium being larger than that of beryllium. In table 2, the larger lattice constant dilation in the [0002] direction as compared to the [10 $\bar{1}$ 3] direction might be attributed to ion-implantation-induced anisotropic strain strength in the  $c$ -axis and  $a$ -axis lattice directions.

20 K PL spectra of as-grown (undoped), as-implanted (Mg implantation), and annealed samples are shown in figure 27 [224]. The band-edge emission ( $\sim 365$  nm) [218] nearly vanishes upon ion implantation. The RTA treatment procedure (1000 °C in N<sub>2</sub> ambient) can only achieve partially recovery of the damaged GaN structure, as discussed in the previous section. As shown by curve (c) of figure 27, the intensity of the band-edge emission is substantially lower than that for undoped GaN samples due to poor crystal quality and/or surface morphology. In addition, 378 nm DA emissions with phonon replicas [220–222] were also observed. In contrast to the case for the as-grown undoped samples, the deep-level emission peak changes position from  $\sim 550$  to  $\sim 528$  nm. According to Ponce *et al* [218], the 356 nm near-band-edge emission was emitted from the large crystallites, while the 550 nm broad yellow band emission was emitted from the low-angle grain boundaries. The activation energy of the 528 nm emission is 16 meV, which is close to the yellow band emission for undoped GaN (15 meV) [223]. It is proposed that the two above-mentioned emissions (the green and yellow emissions) relate to the same DA pair. This result shows that the Mg-ion-induced defect clusters might play a key role in generating green band emission.

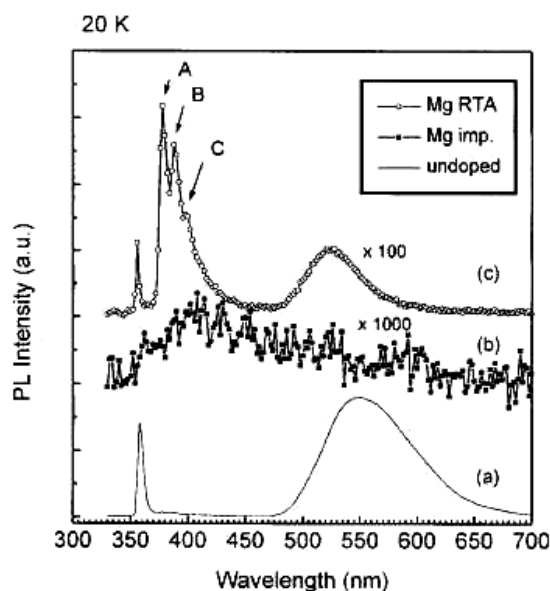


**Figure 27.** 20 K PL spectra of (a) as-grown (undoped), (b) as-implanted (Mg implantation), and (c) annealed samples.

Similar PL phenomena were observed by Pearton and co-workers for  $\text{Si}^+$ -implanted GaN which was annealed under high  $\text{N}_2$  overpressure (15 kbar) [1, 225]. The samples annealed at 1250 and 1400 °C have stronger 378 nm DA emission intensity than the as-grown GaN, but weaker near-band-edge emission intensity. However, the sample annealed at 1500 °C exhibits a stronger band-edge luminescence intensity than the as-grown sample—by a factor of three. Thus, one can propose that the 378 nm DA emission line might be attributable to the defects in the GaN. High-temperature ( $\sim 1500$  °C) annealing can remove more structural damage which results from  $\text{Si}^+$  implantation. Theoretical estimates place the melting temperature of GaN at about 2500 °C (at 4.5 GPa) [18]. This may suggest that the most desirable annealing temperature could be as high as  $\sim 1700$  °C. Strite *et al* have also demonstrated that annealing the Zn-implanted GaN samples near 1500 °C under high  $\text{N}_2$  pressures can enhance the overall luminescence [226]. Suski *et al* [205] also reported that the luminescence efficiency of as-grown GaN samples can be improved by such high-temperature and high-pressure annealing. It was commented that exposure to high-pressure ambient could abate GaN decomposition and enable survival through the 1550 °C high-temperature annealing. In addition, high-pressure annealing and high dislocation densities would strongly affect the Zn diffusion.

As regards n-type implantation doping of GaN, the use of Si and O as n-type dopants has been reported by Zolper *et al* [14, 16, 227]. In addition to nitrogen vacancies, oxygen is a suspected origin of background concentration in as-grown GaN [79]. Owing to its position next to nitrogen in the periodic table, oxygen is a possible alternative n-type dopant. In fact, reports of oxygen incorporation into GaN during growth or implantation have shown oxygen to act as a shallow donor [10, 79–82], as mentioned before. An ionization energy of  $\sim 29$  meV was measured for O-implanted GaN, but a low activation efficiency of  $\sim 3.6\%$  was exhibited. This phenomenon was tentatively attributed to the lighter lattice damage, and therefore generation of vacancies for the lighter O ion or the existence of a second, deeper energy level [14]. The former might result in fewer O atoms occupying the substitutional N sites and therefore one

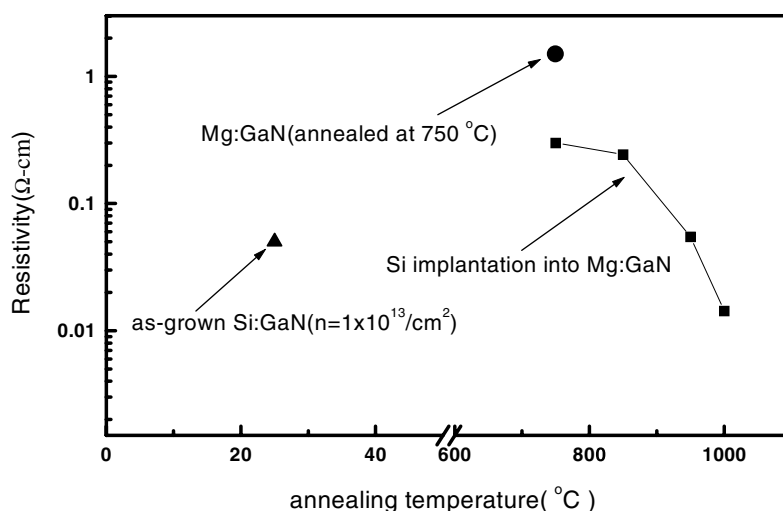
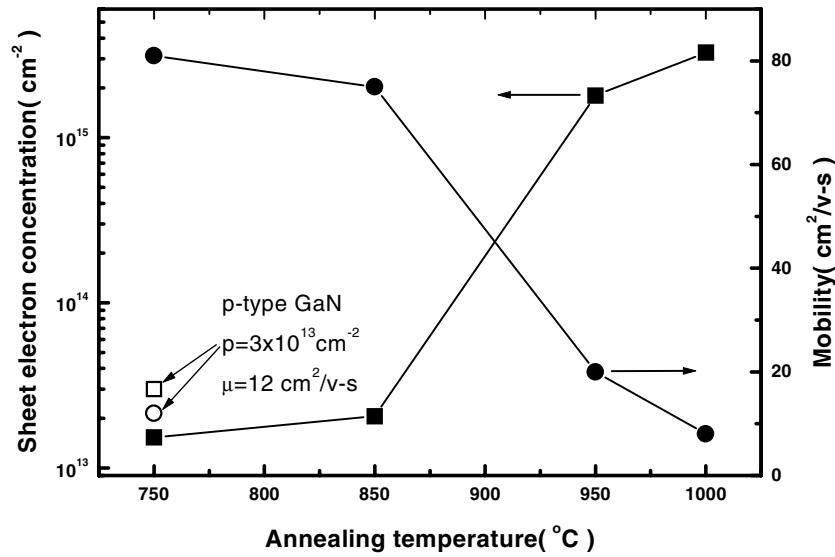


Figure 28. Resistivity of Si-implanted Mg:GaN as a function of annealing temperature.

could not achieve higher activation efficiency. Si implantation in undoped GaN has been demonstrated at a high activation efficiency of 30–50% at a dose of  $1 \times 10^{16} \text{ cm}^{-2}$  [91, 235]. Therefore, the possibility that the electrons generated are due to implantation damage alone rather than Si activation can be discounted by comparing the Si implantation findings to those regarding Ar implantation.

Most studies on ion implantation in GaN have focused on converting the undoped films into n- or the p-type materials. However, n-type GaN created by ion implantation from p-type GaN is still scarce and it would be useful to fabricate the lateral GaN-based p–n junction or the planar bipolar junction transistor on an insulating substrate. Figure 28 shows the resistivity of Si-implanted p-type GaN as a function of annealing temperature [235]. Mg-doped p-type GaN was grown on a *c*-face sapphire substrate by MOVPE [234]. The as-grown Mg-doped GaN films were semi-insulating with resistivity larger than  $10^6 \text{ } \Omega \text{ cm}$ . After thermal annealing in  $\text{N}_2$  at  $750 \text{ } ^\circ\text{C}$ , the resistivity and hole concentration of p-type GaN are around  $1.5 \text{ } \Omega \text{ cm}$  and  $3 \times 10^{17} \text{ cm}^{-3}$ , respectively. Multiple implantation was used to form a uniform Si-implanted layer. The implantation conditions (dose/energy) were  $2 \times 10^{15} \text{ cm}^{-2}/40 \text{ keV}$ ,  $5 \times 10^{15} \text{ cm}^{-2}/100 \text{ keV}$ , and  $5 \times 10^{15} \text{ cm}^{-2}/200 \text{ keV}$ . The overall implanted depth was about  $0.6 \text{ } \mu\text{m}$ , as obtained by TRIM calculation. After ion implantation, the samples underwent  $\text{N}_2$ -ambient thermal annealing between  $700$  and  $1000 \text{ } ^\circ\text{C}$  to achieve recovery of the damaged crystal lattice and to activate the implanted dopant ( $^{28}\text{Si}^+$ ). The annealing time was fixed at 30 min. The as-implanted samples ( $^{28}\text{Si}^+$ -implanted p-type GaN) show near-insulating properties. After  $\text{N}_2$ -ambient thermal annealing, n-type conduction was achieved. The resistivities of the implanted samples exhibit a decreasing trend as the annealing temperatures increase, as shown in figure 28. The lowest resistivity is around  $0.014 \text{ } \Omega \text{ cm}$ , which is two orders of magnitude lower than that for a typical p-type GaN sample. Clearly, Si donors in p-type GaN are efficiently activated after annealing, and convert the top p-type layer to n-type material. However, the resistivity of this Si-implanted n-type GaN is higher than that of as-grown n-type GaN with similar carrier concentration. This might be due to the lower carrier mobility resulting from ion implantation damage. Figure 29 shows the sheet electron concentration ( $N_s$ ) and Hall mobility as functions of annealing temperature.  $N_s$  increases with increasing annealing temperature. In other words, the activation efficiency varied from 0.4 to 27% with the annealing temperature  $f$  varying from



**Figure 29.** The sheet electron concentration ( $N_s$ ) and Hall mobility of Si-implanted Mg:GaN as functions of annealing temperature.

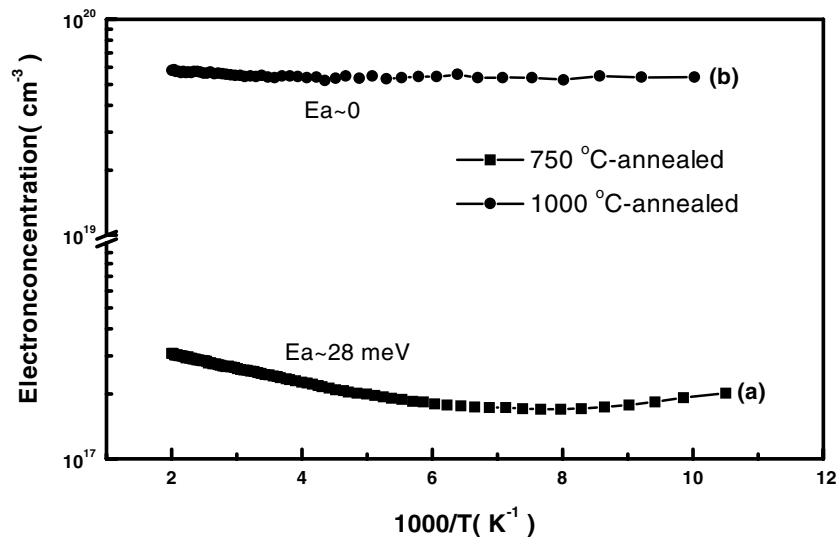


**Figure 30.** Temperature-dependent Hall measurements for Si-implanted Mg:GaN annealed at (a) 750 °C and (b) 1000 °C.

750 to 1000 °C. The highest  $N_s$  for Si-implanted p-type GaN was around  $3 \times 10^{15} \text{ cm}^{-2}$ , which corresponds to a carrier concentration of  $5 \times 10^{19} \text{ cm}^{-3}$  at room temperature, when the sample was annealed at a temperature of 1000 °C for 30 min. In this study, the annealing temperatures were kept below 1000 °C so as to avoid severe surface dissociation occurring in the samples. As regards the samples annealed at 750 °C, from the slope of the plot of the carrier concentration versus the reciprocal temperature shown as curve (a) of figure 30, an ionization energy of  $\sim 28 \text{ meV}$  was obtained. This value is close to the previous reports [10–12, 74, 75].

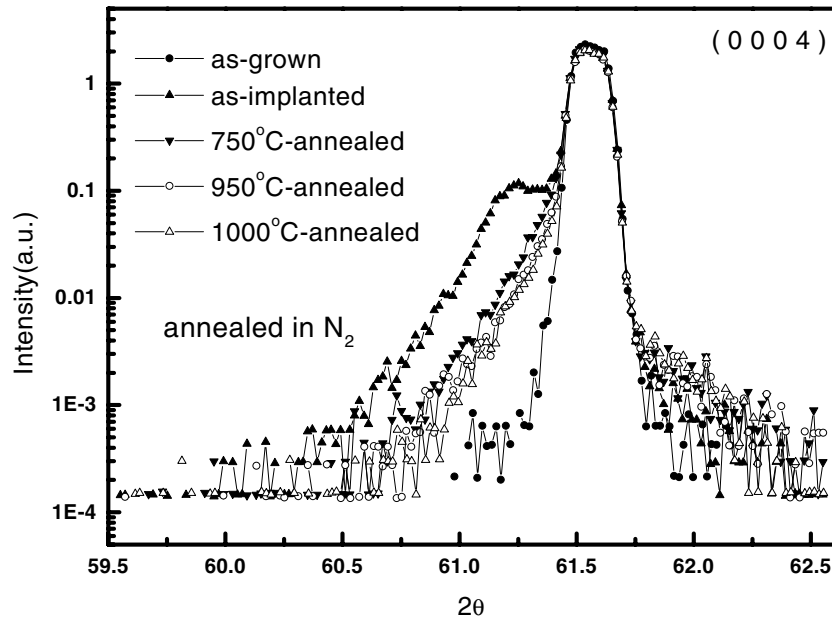
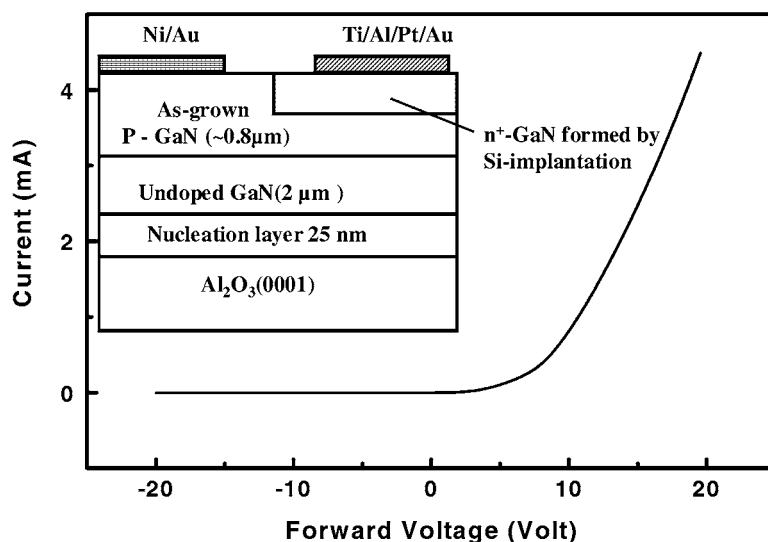


Figure 31. X-ray diffraction spectra of Si-implanted Mg:GaN taken in the [0004] direction.

At high temperature the sample exhibits the typical thermally activated electron concentration profile. The electron concentration decreases with reduction of the measured temperature, but when the temperature is lower than 150 K, the electron concentration appears to increase again, indicating the onset of impurity band conduction. However, the electron concentration of the sample annealed at 1000 °C is maintained at approximately  $5 \times 10^{19} \text{ cm}^{-3}$  even at low temperature, as shown by curve (b) of figure 30. Therefore, the ionization energy was near zero for the sample annealed at 1000 °C. In other words, electron concentration is independent of temperature. This phenomenon is usually observed for highly doped semiconductors, since the impurity band widens and merges with the conduction band [158]. As shown in figure 29, the mobility of Si-implanted p-type GaN samples decreases as the annealing temperature increases. This phenomenon may be understood as a result of the probability of electron scattering increasing with increasing ionized Si impurity concentration. Zolper *et al* [227] reported that Si implantation ( $5 \times 10^{15} \text{ cm}^{-2}/100 \text{ keV}$ ) in GaN can reach 35% activation at an annealing temperature of 1100 °C. They showed that significant implantation damage remains even after high-temperature annealing and the activation of Si atoms seems to be insensitive to implantation damage [227]. In other words, effective recovery of the damaged lattice could not be achieved by means of thermal annealing with temperature around 1100 °C. Figure 31 shows the x-ray data for Si-implanted p-type GaN. Before thermal annealing the samples clearly show a two-layer structure which consists of an Si-implanted layer and an as-grown layer [235]. After thermal annealing, the damaged lattice showed partially recovery, as shown in figure 31. Although the electrical properties of the annealed samples show a significant improvement when better recovery towards the as-grown form of GaN is achieved, the x-ray data show that significant lattice distortion remains even after annealing at 1000 °C. Cao *et al* [228] observed that the distorted lattice of high-dose Si-implanted GaN could be recovered at annealing temperatures above 1300 °C. However, at this high temperature protection of the surface may be imperative. It is well known that ion implantation would induce anisotropic



**Figure 32.** The current–voltage ( $I$ – $V$ ) characteristic of a GaN  $n^+$ – $p$  junction created by  $^{28}\text{Si}^+$  implantation into Mg-doped GaN. The inset shows schematically the structure of a GaN  $n^+$ – $p$  junction.

strain strength in the various lattice directions. Implantation of atoms of larger size and at higher dose would induce larger lattice constant dilation. High  $\text{N}_2$  pressures may be needed for annealing above  $1300^\circ\text{C}$  to remove the implantation-induced damage in GaN and prevent the GaN surface from undergoing severe dissociation.

Although the mobility of Si-implanted p-type GaN is still smaller than that of MOVPE-grown Si-doped GaN with the same carrier concentration,  $n^+$ -type GaN has been successfully created by Si implantation into p-type GaN. One can expect creation of GaN  $n^+$ – $p$  junctions to be simpler to achieve than that of GaN  $p^+$ – $n$  junctions, because of the lower activation efficiency of p-type implants. Such creation will enable lateral GaN-based bipolar junction transistors to be produced on an insulating substrate. Figure 32 shows the current–voltage ( $I$ – $V$ ) characteristic of a GaN  $n^+$ – $p$  junction created by  $^{28}\text{Si}^+$  implantation into Mg-doped GaN, followed by thermal annealing at  $1000^\circ\text{C}$  in  $\text{N}_2$  ambient [235]. The inset of figure 32 shows schematically the structure of the GaN  $n^+$ – $p$  junction. The n-type electrode was made using Ti/Al/Pt/Au metal contacts, while the p-type electrode was made using Ni/Au metal contacts. The switch-on voltage and series resistance of the implanted p–n junctions are far larger than those of as-grown p–n junctions. These poor electrical properties of implanted  $n^+$ – $p$  junctions could be attributable to the severe surface dissociation that occurs during high-temperature annealing, resulting in poor p-type ohmic contacts.  $\rho_c$  of n-type contacts can be as low as  $1.5 \times 10^{-6} \Omega \text{ cm}^2$ , when a Ti/Al/Pt/Au metal contact is annealed in  $\text{N}_2$  ambient at  $600^\circ\text{C}$  [229]. Therefore, optimizing the annealing process is expected to be important for further improving the electrical performance of implanted  $n^+$ – $p$  junctions.

## 5. Summary

For GaN-based materials, problems of epitaxial defects and p-type doping combine together, and they play a key role in realizing high-efficiency optoelectronic devices, such as laser diodes, LEDs, and heterojunction bipolar transistors. The doping process is substantially

affected by grown-in defects and unintentional introduction of impurities, which may cause self-compensation. The understanding of the nature of the incorporation of p-type dopants is important for the control of p-type doping in GaN. Theoretical prediction suggested that the thermal activation energy for Be is much smaller than for Mg; however, up to now, low-resistivity p-type GaN has only been achieved by using Mg as the p-type dopant. Despite production of p-type Be-doped GaN having been demonstrated, consistent data are still too sparse to allow practical device implementation. According to the theoretical calculations and a few experiments, use of Ca might also be possible to achieve p-type GaN doping. How to use inherent properties to optimize p-type doping in GaN is one of the most crucial issues for the future development of nitride semiconductor devices, especially for UV-based lighting sources. In addition, the silicon-implantation-generated GaN n<sup>+</sup>-p junctions could be promising as regards future device technology development.

### Acknowledgments

The authors would like to thank C C Lee, C J Pan, M S Tsai, C J Tun and M L Lee for their assistance in the collection of related literature.

### References

- [1] Pearton S J, Zolper J C, Sheu R J and Ren F 1999 *J. Appl. Phys.* **86** 1 and references therein
- [2] Amano H, Kito M, Hiramatsu K and Akasaki I 1989 *Japan. J. Appl. Phys.* **28** L2112
- [3] Nakamura S, Mukai T and Senoh M 1991 *Japan. J. Appl. Phys.* **31** L139
- [4] Kumakura K and Kobayashi N 1999 *Japan. J. Appl. Phys.* **38** L1012
- [5] Kozodoy P, Hansen M, DenBaars S P and Mishra U K 1999 *Appl. Phys. Lett.* **74** 3681
- [6] Kozodoy I P, Smorchkova Y P, Hansen M, Xing H, DenBaars S P, Mishra U K, Saxler A W, Perrin R and Mitchel W C 1999 *Appl. Phys. Lett.* **75** 2444
- [7] Koide N *et al* 1991 *J. Cryst. Growth.* **115** 639
- [8] Nakamura S, Mukai T and Senoh M 1992 *Japan. J. Appl. Phys.* **31** 2883
- [9] Murakami H *et al* 1991 *J. Cryst. Growth* **115** 648
- [10] Lee I H *et al* 1997 *J. Cryst. Growth* **182** 314
- [11] Fistul V I 1969 *Heavily Doped Semiconductors* (New York: Plenum) p 26
- [12] Wickenden A E, Rowland L B, Doverspike K, Gaskill D K, Freitas J A Jr, Simons N D S and Chi P H 1995 *J. Electron. Mater.* **24** 1547
- [13] Pankove J I and Hutchby J A 1974 *Appl. Phys. Lett.* **24** 281
- [14] Pankove J I and Hutchby J A 1976 *J. Appl. Phys.* **47** 5387
- [15] Pearton S J, Abernathy C R, Vartuli C B, Zolper J C, Yuan C and Stall R A 1995 *Appl. Phys. Lett.* **67** 1435
- [16] Zolper J C, Wilson R G, Pearton S J and Stall R A 1996 *Appl. Phys. Lett.* **68** 1945
- [17] Edgar J H 1994 *Properties of Group III Nitrides* (London: INSPEC) p 273
- [18] Van Vechten J A 1973 *Phys. Rev. B* **7** 1479
- [19] Karpinski J, Jun J and Porowski S 1984 *J. Cryst. Growth* **66** 1
- [20] Maruska H P and Tietjen J J 1969 *Appl. Phys. Lett.* **15** 327
- [21] Perlin P *et al* 1995 *Phys. Rev. Lett.* **75** 296
- [22] Zhang G Y, Tong Y Z, Yang Z J, Jin S X, Li J and Gan Z Z 1997 *Appl. Phys. Lett.* **71** 3376
- [23] Neugebauer J and Van de Walle C G 1996 *Appl. Phys. Lett.* **69** 503
- [24] Gotz W, Johnson N M, Chen C, Liu H, Kuo C and Imler W 1996 *Appl. Phys. Lett.* **68** 3144
- [25] Perlin P, Suzuki T, Teisseyre H, Leszczynski M, Gregory I and Jun J 1997 *Mater. Res. Soc. Symp. Proc.* **449** 519
- [26] Gotz W, Walker J, Romano L T and Johnson N M 1997 *Mater. Res. Soc. Symp. Proc.* **449** 525
- [27] di Forte-Poisson M A *et al* 1998 *J. Cryst. Growth* **195** 314
- [28] Ploog K H and Brandt O 1998 *J. Vac. Sci. Technol. A* **16** 1609
- [29] Gotz W *et al* 1999 *Mater. Sci. Eng. B* **59** 211
- [30] Boguslawski P, Briggs E L and Bernholc J 1995 *Phys. Rev. B* **51** 17 255
- [31] Kim W, Botchkarev A E, Salvador A, Popovici G, Tang H and Morkoc H 1997 *J. Appl. Phys.* **82** 219

- [32] Shan W, Ager J W III, Walukiewicz W, Haller E E, Little B D, Song J J, Schurman M, Feng Z C, Stall R A and Goldenberg B 1998 *Appl. Phys. Lett.* **72** 2274 and the references therein
- [33] Van de Walle C G 1998 *Phys. Rev. B* **57** 2033
- [34] Yoshida S, Misawa S and Gonda S 1982 *J. Appl. Phys.* **53** 6844
- [35] Khan M A, Skogman R A, Schulze R G and Gershenzon M 1983 *Appl. Phys. Lett.* **43** 492
- [36] Koide Y, Itoh H, Sawaki N, Akasaki I and Hashimoto M 1986 *J. Electrochem. Soc.* **133** 1956
- [37] Redwing J M, Flynn J S, Tischler M A, Michel W and Saxler A 1996 *Mater. Res. Soc. Symp. Proc.* **395** 201
- [38] Shin M, Polyakov A Y, Skowronski M, Greve D W, Wilson R G and Freitas J A 1996 *Mater. Res. Soc. Symp. Proc.* **423** 643
- [39] Polyakov A Y, Shin M, Pearton S J, Skowronski M, Greve D W and Freitas J A 1996 *Mater. Res. Soc. Symp. Proc.* **423** 607
- [40] Amano H, Sawaki N, Akasaki I and Toyoda T 1986 *Appl. Phys. Lett.* **48** 353
- [41] Nakamura S 1991 *Japan. J. Appl. Phys.* **30** L1705
- [42] Lin C F, Cheng H C, Chi G C, Feng M S, Guo J D, Hong J M and Chen C Y 1997 *J. Appl. Phys.* **82** 2378
- [43] Lin C F, Cheng H C, Feng M S and Chi G C 1998 *Mater. Sci. Eng. B* **50** 25
- [44] Lin C F, Chi G C, Feng M S, Guo J D, Tsang T S and Hong J M 1996 *Appl. Phys. Lett.* **68** 3758
- [45] Lee C H, Chi G C, Lin C F, Feng M S and Guo J D 1996 *Appl. Phys. Lett.* **68** 3440 and references therein
- [46] Nakamura S, Mukai T and Senoh M 1991 *Japan. J. Appl. Phys.* **30** L1998
- [47] Spitzer W G and Panish M B 1969 *J. Appl. Phys.* **40** 4200
- [48] Shimazu M, Kamon K, Kimura K, Mashida M, Mihara M and Ishii M 1987 *J. Cryst. Growth* **83** 327
- [49] Hotta H, Hino I and Suzuki T 1988 *J. Cryst. Growth* **93** 618
- [50] Druminsky M, Wolf H D and Zschauer K H 1982 *J. Cryst. Growth* **57** 318
- [51] Nakamura S, Mukai T and Senoh M 1992 *J. Appl. Phys.* **71** 5543
- [52] Mott N F and Twose T D 1961 *Adv. Phys.* **10** 107
- [53] Molnar R J, Lei T and Moustakas T D 1993 *Appl. Phys. Lett.* **62** 72
- [54] Sheu J K and Chi G C unpublished results
- [55] Gotz W, Johnson N M, Walker J, Bour D P and Street R A 1996 *Appl. Phys. Lett.* **68** 667
- [56] Malik R J *et al* 1993 *J. Cryst. Growth* **127** 686
- [57] Zhang D H, Radhakrishnan K and Yoon S F 1995 *J. Cryst. Growth* **148** 34
- [58] Grieshaber W, Schubert E F, Goepfert I D, Karlicek R F Jr, Schurman M J and Tran C 1996 *J. Appl. Phys.* **80** 4615
- [59] Monemar B 1974 *Phys. Rev. B* **10** 676
- [60] Shan W, Schmidt T J, Yang X H, Hwang S J, Song J J and Goldberg B 1995 *Appl. Phys. Lett.* **66** 985
- [61] Calderon L, Lu Y, Shen H, Pamulapati J, Dutta M, Chang W H, Yang L W and Wright P D 1992 *Appl. Phys. Lett.* **60** 1597
- [62] De-Sheng J D, Makita Y, Ploog K and Queisser H J 1982 *J. Appl. Phys.* **53** 999
- [63] Moustakas T D, Molnar R, Lei T, Menon G and Eddy C R 1992 *Wide Band Gap Semiconductors (MRS Soc. Symp. Proc. vol 242)* ed T D Moustakas, J I Pankove and Y Hamakawa (Pittsburgh, PA: Materials Research Society) pp 427–32
- [64] Weinmann N G, Eastman L F, Doppalapudi D, Ng H M and Moustakas T D 1998 *J. Appl. Phys.* **83** 3656
- [65] Iliopoulos E, Doppalapudi D, Ng H M and Moustakas T D 1998 *Appl. Phys. Lett.* **73** 375
- [66] Oh E, Park H and Park Y 1998 *Appl. Phys. Lett.* **72** 1848
- [67] Jacob G, Boulou M and Furtado M 1977 *J. Cryst. Growth* **42** 136
- [68] Morgan T N 1965 *Phys. Rev.* **139** A343
- [69] Nakamura S and Fasol G 1997 *The Blue Laser Diode* (Berlin: Springer) p 97
- [70] Schubert E F, Goepfert I D, Grieshaber W and Redwing J M 1997 *Appl. Phys. Lett.* **71** 921
- [71] Ogino T and Aoki M 1980 *Japan. J. Appl. Phys.* **19** 2395
- [72] Zhang X, Kung P, Walker D, Saxler A and Razeghi M 1996 *Mater. Res. Soc. Symp. Proc.* **395** 625
- [73] Hoffmann H *et al* 1997 *Solid-State Electron.* **41** 275
- [74] Tanaka T, Watanabe A, Amano H, Kobayashi H, Akasaki I, Yamasaki S and Koike M 1994 *Appl. Phys. Lett.* **65** 2024
- [75] Neugebauer J and Van de Walle C G 1994 *Phys. Rev. B* **50** 8067
- [76] Guo J D, Feng M S and Pang F M 1995 *Japan. J. Appl. Phys.* **34** 5510
- [77] Yi G C and Wessels B W 1996 *Appl. Phys. Lett.* **69** 3028
- [78] Korotkov R Y and Wessels B W 1999 *Mater. Res. Soc. Symp. Proc.* **595** 3.80.1
- [79] Chung B C and Gershenzon M 1992 *J. Appl. Phys.* **72** 651
- [80] Chen W M *et al* 1998 *Phys. Rev. B* **58** R13351
- [81] Joshkin V A *et al* 1998 *J. Appl. Phys.* **86** 281

- [82] Niebuhr R *et al* 1997 *J. Electron. Mater.* **26** 1127
- [83] Zolper J C, Wilson R G, Pearton S J and Stall R A 1996 *Appl. Phys. Lett.* **68** 1945
- [84] Khan M A, Schulze R G and Gershenson M 1983 *Appl. Phys. Lett.* **43** 492
- [85] Yoshida S, Misawa S and Gonda S 1982 *J. Appl. Phys.* **53** 6844
- [86] Lee H G, Gershenson M and Goldenberg B L 1991 *J. Electron. Mater.* **20** 621
- [87] Bremser M D, Perry W G, Zheleva T, Edwards N V, Nam O H, Parikh N, Aspens D E and Davis R F 1996 *J. Nitride Semicond. Res.* **1** 8
- [88] Stampfl C and Van de Walle C G 1998 *Appl. Phys. Lett.* **72** 459
- [89] Polyakov A Y, Shin M, Freitas J A, Skowronski M, Greve D W and Wilson R G 1996 *J. Appl. Phys.* **80** 6349
- [90] Korakakis D, Ng H M, Ludwig K F Jr and Moustakas T D 1997 *Mater. Res. Soc. Symp. Proc.* **449** 233
- [91] Yoshimoto N, Matsuoka T and Katsui A 1991 *Appl. Phys. Lett.* **9** 2251
- [92] Matsuoka T, Yoshimoto N, Sasaki T and Katsui A 1992 *J. Electron. Mater.* **21** 157
- [93] Abernathy C R, Pearton S J, Fen R and Wisk P W 1993 *J. Vac. Sci. Technol. B* **11** 179
- [94] MacKenzie J D, Abernathy C R, Stewart J D and Muhr G T 1996 *J. Cryst. Growth* **164** 143
- [95] Abernathy C R, MacKenzie J D, Bharatan S R, Jones K S and Pearton S J 1995 *Appl. Phys. Lett.* **66** 1632
- [96] Nakamura S, Iwasa N and Nagahama S 1993 *Japan. J. Appl. Phys.* **32** L338
- [97] Nakamura S, Mukai T and Senoh M 1993 *Japan. J. Appl. Phys.* **32** L16
- [98] Nakamura S and Fasol G 1997 *The Blue Laser Diode* (Berlin: Springer) p 139
- [99] Ilegems M, Dingle R and Logan R A 1972 *J. Appl. Phys.* **43** 3797
- [100] Pankove J I and Hutchby J A 1974 *Appl. Phys. Lett.* **24** 281
- [101] Nakamura S, Senoh M, Nagahama S, Iwasa N, Yamada T, Matsushita T, Sugimoto Y and Kiyoku H 1997 *Appl. Phys. Lett.* **70** 1417
- [102] Keller S, Abare A C, Minsky M S, Wu X H, Mack M P, Speck J S, Hu E, Coldren L A, Mishra U K and DenBaars S P 1998 *Mater. Sci. Forum* **264–8** 1157
- [103] Bidnyk S, Schmidt T J, Cho Y H, Gainer G H, Song J J, Keller S, Mishra U K and DenBaars S P 1998 *Appl. Phys. Lett.* **72** 1623
- [104] Chichibu S F *et al* 1998 *Appl. Phys. Lett.* **73** 2006
- [105] Chichibu S F, Sota T, Wada K, DenBaars S P and Nakamura S 1999 *MRS Internet J. Nitride Semicond. Res.* **4** S1 G.2.7
- [106] Cho Y H, Song J J, Keller S, Minsky M S, Hu E, Mishra U K and DenBaars S P 1998 *Appl. Phys. Lett.* **73** 1128
- [107] Keller S, Chichibu S F, Minsky M S, Hu E, Mishra U K and DenBaars S P 1998 *J. Cryst. Growth* **195** 258
- [108] Zeng K C, Lin J Y, Jiang X, Salvador A, Popovici G, Tang H, Kim W and Morkoc H 1997 *Appl. Phys. Lett.* **71** 1638
- [109] Ruvimov S, Liliental-Weber Z, Suski T, Ager J W III, Washburn J, Krueger J, Kisielwski C, Weber E R, Amano H and Akasaki I 1996 *Appl. Phys. Lett.* **69** 990
- [110] Nakamura S and Fasol G 1997 *The Blue Laser Diode* (Berlin: Springer) p 177
- [111] Neugebauer J and Van de Walle C G 1995 *Phys. Rev. Lett.* **75** 4452
- [112] Ohba Y and Hatano A 1994 *Japan. J. Appl. Phys.* **33** L1367
- [113] Tasi T L, Chang A Y, Chang C L, Sung C S, Jong C S, Chen T P and Huang K H 2000 *IWN2000: Int. Workshop on Nitride Semiconductors (Nagoya, Japan, Sept. 2000)*
- [114] Lai W C, Yokoyama M, Guo J D, Sze S M, Sheu C H, Chen T Y and Chang S H 2000 *IWN2000: Int. Workshop on Nitride Semiconductors (Nagoya, Japan, Sept. 2000)*
- [115] Neugebauer J and Van de Walle C G 1996 *Mater. Res. Soc. Symp. Proc.* **395** 645
- [116] Reboledo F A and Pantelides S T 1999 *Phys. Rev. Lett.* **82** 1887
- [117] Van Vechten J A, Zook J D, Hornig R D and Goldenberg B 1992 *Japan. J. Appl. Phys.* **31** 3662
- [118] Neugebauer J and Van de Walle C G 1996 *Appl. Phys. Lett.* **69** 503
- [119] Kim W, Salvador A, Botchkarev A E, Aktas O, Mohammad S N and Morkoc H 1996 *Appl. Phys. Lett.* **69** 559
- [120] Sugiura L, Suzuki M and Nishio J 1998 *Appl. Phys. Lett.* **72** 1748
- [121] Sheu J K, Su Y K, Chi G C, Chen W C, Chen C Y, Hung C N, Hong J M, Yu Y C, Wang C W and Lin E K 1998 *J. Appl. Phys.* **83** 3172
- [122] Bour D P *et al* 1997 *Mater. Res. Soc. Symp. Proc.* **449** 509
- [123] Kaufmann U, Schlotter P, Obloh H, Kohler K and Maier M 2000 *Phys. Rev. B* **62** 10 867
- [124] Amano H, Kito M, Hiramatsu K and Akasaki I 1990 *J. Electrochem. Soc.* **137** 1639
- [125] Maruska H P and Tietjen J J 1969 *Appl. Phys. Lett.* **15** 367
- [126] Strite S and Morkoc H 1992 *J. Vac. Sci. Technol. B* **10** 1237
- [127] Nakamura S, Mukai T, Senoh M and Iwasa N 1992 *Japan. J. Appl. Phys.* **31** L139
- [128] Myoung J M, Shim K H, Kim C, Kim K, Kim S and Bishop S G 1996 *Appl. Phys. Lett.* **69** 2722
- [129] Strite S and Morkoc H 1992 *J. Vac. Sci. Technol. B* **10** 1237

- [130] Hong C H, Pavidis D and Brown S W 1995 *J. Appl. Phys.* **74** 1705
- [131] Dingle R and Ilegems M 1971 *Solid State Commun.* **9** 175
- [132] Viswanath A K, Shin E, Lee J I, Yu S, Kim D, Kim B, Choi Y and Hong C H 1998 *J. Appl. Phys.* **83** 2272
- [133] Shahedipour F and Wessels B W 2000 *Appl. Phys. Lett.* **76** 3011
- [134] Kaufmann U *et al* 1998 *Appl. Phys. Lett.* **72** 1326
- [135] Smith M, Chen G D, Lin J Y, Jiang H X, Salvador A, Sverdlov B N, Botchkarev A, Morkoc H and Goldenberg B 1996 *Appl. Phys. Lett.* **68** 1883
- [136] Morkoc H *et al* 1995 *1st Int. Conf. on GaN and Related Compounds (MRS Fall Mtg) (Boston, MA, Nov. 1995)* (Pittsburgh, PA: Materials Research Society)
- [137] Pankove J I 1971 *Optical Processes in Semiconductors* (Englewood Cliffs, NJ: Prentice-Hall) pp 147–52
- [138] Reshchikov M, Yi G-C and Wessels B W 1999 *Phys. Rev. B* **59** 13 176
- [139] Oh E, Park H and Park Y 1998 *Appl. Phys. Lett.* **72** 70  
Sheu J K, Su Y K, Chi G C, Pong B J, Chen C Y, Huang C N and Chen W C 1998 *J. Appl. Phys.* **84** 4590
- [140] Reshchikov M, Yi G-C and Wessels B W 1999 *MRS Internet J. Nitride Semicond. Res.* **4** S1 G11.8
- [141] Shklovskii B I and Eforos A L 1984 *Electronic Properties of Doped Semiconductors* (Berlin: Springer) p 52
- [142] Casey H C Jr, Muth J, Krishnankutty S and Zavada J M 1996 *Appl. Phys. Lett.* **68** 2867
- [143] Gotz W, Johnson N M, Amano H and Akasaki I 1994 *Appl. Phys. Lett.* **65** 463
- [144] Brandt O, Yang H, Kostial H and Ploog K H 1996 *Appl. Phys. Lett.* **69** 2707
- [145] Salvador A, Kim W, Botchkarev A, Fan Z and Morkoc H 1996 *Appl. Phys. Lett.* **69** 2692
- [146] Ronning C, Carlson E P, Thomson D B and Davis R F 1998 *Appl. Phys. Lett.* **73** 1622
- [147] Bernardini F and Fiorentini V 1997 *Appl. Phys. Lett.* **70** 2992
- [148] Neugebauer J and Van de Walle C G 1999 *J. Appl. Phys.* **85** 3003
- [149] Kim K S, Han M S, Yang G M, Youn C J and Lee H J 2000 *Appl. Phys. Lett.* **77** 1123
- [150] Wilson R G, Pearton S J, Abernathy C R and Zavada J M 1995 *Appl. Phys. Lett.* **66** 2238
- [151] Kuznetsov N I, Nikolaev A E, Zubrilov A S, Melnik Yu V and Dmitriev V A 1999 *Appl. Phys. Lett.* **75** 3138
- [152] Tang H, Webb J B, Bardwell J A, Raymond S, Salzman J and Uzan-Saguy C 2001 *Appl. Phys. Lett.* **78** 757
- [153] Webb J B, Tang H, Rolfe S and Bardwell J A 1999 *Appl. Phys. Lett.* **75** 953
- [154] Zhang R and Kuech T F 1998 *Appl. Phys. Lett.* **72** 1611
- [155] Fischer S, Wetzell C, Haller E E and Meyer B K 1995 *Appl. Phys. Lett.* **67** 1298
- [156] Kozodoy P, Xing H, DenBaars S P, Mishra U K, Perrin A S R, Elhamri S and Mitchel W C 2000 *J. Appl. Phys.* **87** 1832
- [157] Tanaka T, Watanabe A, Amano H, Kobayashi Y, Akasaki I, Yamasaki S and Koike M 1994 *Appl. Phys. Lett.* **65** 593
- [158] Mott N F 1990 *Metal-Insulator Transitions* (London: Taylor and Francis)
- [159] Huang J W, Kuech T F, Lu H Q and Bhat I 1996 *Appl. Phys. Lett.* **68** 2392
- [160] Johnson C, Lin J Y, Jiang H X, Khan M A and Sun C J 1996 *Appl. Phys. Lett.* **68** 1808
- [161] Seghier D and Gislason H P 2000 *J. Appl. Phys.* **88** 6483
- [162] Miyachi M, Tanaka T, Kimura Y and Ota H 1998 *Appl. Phys. Lett.* **72** 1101
- [163] Hull B A, Mohny S E, Venugoplan H S and Ramer J C 2000 *Appl. Phys. Lett.* **76** 2271
- [164] Koide Y, Maeda T, Kawakami T, Fujita S, Uemura T, Shibata N and Murakami M 1999 *J. Electron. Mater.* **28** 341
- [165] Ho J K, Jong C S, Chiu C C, Huang C N, Shih K K, Chen L C, Chen F R and Kai J J 1998 *J. Appl. Phys.* **86** 4491
- [166] Chen L C, Chen F R, Kai J J, Ho J K, Jong C S, Chiu C C, Huang C N and Shih K K 1999 *J. Appl. Phys.* **86** 3862
- [167] Pearton S J, Cho H, LaRoche J R, Ren F, Wilson R G and Lee J W 1999 *J. Appl. Phys.* **75** 2939
- [168] Chang S J, Su Y K, Tsai T L, Chang C Y, Chiang C L, Chang C S, Chen T P and Huang K H 2001 *Appl. Phys. Lett.* **78** 312
- [169] Lai W C, Yokoyama M, Chang S J, Guo J D, Sheu C H, Chen T Y, Tsai W C, Tsang J S, Chan S H and Sze S M 2000 *Japan. J. Appl. Phys.* **39** L1138
- [170] Takeya M and Ikeda M 2000 *Proc. Int. Workshop on Nitride Semiconductors (IPAP Conf. Ser. 1)* p 746
- [171] Van de Walle C G, Stampfl C and Neugebauer J 1998 *J. Cryst. Growth* **189** 505
- [172] Mattila T and Nieminen R M 1997 *Phys. Rev. B* **55** 9571
- [173] Mattila T and Nieminen R M 1996 *Phys. Rev. B* **54** 16 676
- [174] Van de Walle C G, Stampfl C, Neugebauer J, McCluskey M D and Johnson N M 1999 *MRS Internet J. Nitride Semicond. Res.* **4** S1 G10.4
- [175] Suzuki M, Nishio J, Onomura M and Hongo C 1998 *J. Cryst. Growth* **188/189** 511
- [176] Gotz W, Johnson N M, Walker J, Bour D P, Amano H and Akasaki I 1995 *Appl. Phys. Lett.* **67** 2666

- [177] Dingle R, Stormer H L, Gossard A C and Wiegmann W 1978 *Appl. Phys. Lett.* **33** 665
- [178] Bergman J P, Zhao Q X, Holtz P O, Monemar B, Sundaram M, Merz J L and Gossard A C 1991 *Phys. Rev. B* **43** 4771
- [179] Su L and Walukiewicz W 1999 *Appl. Phys. Lett.* **74** 2405
- [180] Saxler A, Mitchel W C, Kung P and Razeghi M 1999 *Appl. Phys. Lett.* **74** 2023
- [181] Sheu J K, Su Y K, Chi G C, Jou M J, Chang C M, Liu C C and Hung W C 1999 *Appl. Phys. Lett.* **74** 2340
- [182] Ho J-K, Jong C-S, Chiu C C, Huang C-N, Chen C-Y and Shih K-K 1999 *Appl. Phys. Lett.* **74** 1275
- [183] Jang J-S, Chang I-S, Kim H-K, Seong T-Y, Lee S and Park S-J 1999 *Appl. Phys. Lett.* **74** 70
- [184] Jang J-S and Seong T-Y 2000 *Appl. Phys. Lett.* **76** 2742
- [185] Li Y-L, Schubert E F, Graff J W, Osinsky A and Schaff W F 2000 *Appl. Phys. Lett.* **76** 2728
- [186] Yamasaki S, Asami S, Shibata N, Koike M, Manabe K, Tanaka T, Amano H, and Akasaki I 1995 *Appl. Phys. Lett.* **66** 1112
- [187] Lee C R, Son S J, Lee I H, Leem J Y and Noh S K 1997 *J. Cryst. Growth* **182** 6
- [188] Lee C R, Leem J Y, Son S J, Noh S K, Lee I H and Leem K Y 1999 *J. Cryst. Growth* **197** 6
- [189] Reverchon J-L, Huet F, Poisson M-A and Duboz J-Y 2000 *J. Appl. Phys.* **88** 5138
- [190] Amano H, Koike M, Hiramatsu K and Akasaki I 1990 *J. Electrochem. Soc.* **137** 1639
- [191] Kumakura K, Makimoto T and Kobayashi N 2000 *Japan. J. Appl. Phys.* **39** L337
- [192] Akasaki I and Amano H 1997 *Japan. J. Appl. Phys.* **36** 5393
- [193] Kumakura K, Makimoto T and Kobayashi N 2000 *Japan. J. Appl. Phys.* **39** L195
- [194] Manz Ch, Kunzer M, Obloh H, Ramakrishnan A and Kaufmann U 1999 *Appl. Phys. Lett.* **74** 3993
- [195] Rubin M, Newman N, Chan J S, Fu T C and Ross J T 1994 *Appl. Phys. Lett.* **64** 64
- [196] Yang Y-J, Yen J-L, Yang F-S and Lin C-Y 2000 *J. Japan. Appl. Phys.* **39** L390
- [197] Pan C J and Chi G C 1999 *Solid-State Electron.* **43** 621
- [198] Chi G C, Kuo C H, Sheu J K and Pan C J 2000 *Mater. Sci. Eng. B* **75** 210
- [199] Dingle R, Sell D D, Stokowski S E and Ilegems M 1971 *Phys. Rev. B* **4** 1211
- [200] Götz W, Johnson N M, Street R A, Amano H and Akasaki I 1995 *Appl. Phys. Lett.* **66** 1340
- [201] Šantic B, Merz C, Kaufmann U, Niebuhr R, Obloh H and Bachem K 1997 *Appl. Phys. Lett.* **71** 1837
- [202] Solkowski E, Pomrenke G S, Yeo Y K and Hengehold R L 1997 *Phys. Scr. T* **69** 276
- [203] Pearton S J, Cho H, LaRoche J R, Ren F, Wilson R G and Lee J W 1999 *Appl. Phys. Lett.* **75** 2939
- [204] Lin C F, Cheng H C, Chi G C, Bu C J and Feng M S 2000 *Appl. Phys. Lett.* **76** 1878
- [205] Suski T, Jun J, Leszczynski M, Teisseyre H, Strite S, Rockett A, Pelzmann A, Kamp M and Ebeling K J 1998 *J. Appl. Phys.* **84** 1155
- [206] Bernardini F, Fiorentini V and Bosin A 1997 *Appl. Phys. Lett.* **70** 2990
- [207] Brandt O, Yang H, Kostial H and Ploog K H 1996 *Appl. Phys. Lett.* **69** 2707
- [208] Salvador A, Kim W, Aktas O, Botchkarev A, Fan Z and Morkoc H 1996 *Appl. Phys. Lett.* **69** 2692
- [209] Cheng T S, Foxon C T, Jenkins L C, Hooper S E, Lacklison D E, Orton J W, Ber B Y, Merkulov A V and Novikov S V 1996 *Semicond. Sci. Technol.* **11** 538
- [210] Ronning C, Carlson E P, Thomson D B and Davis R F 1998 *Appl. Phys. Lett.* **73** 1622
- [211] Wilson R G, Pearton S J, Abernathy C R and Zavada J M 1995 *Appl. Phys. Lett.* **66** 2238
- [212] Wilson R G, Vartuli C B, Pearton S J, Abernathy C R and Zavada J M 1995 *Solid-State Electron.* **38** 1329
- [213] Strite S 1994 *Japan. J. Appl. Phys.* **33** L699
- [214] Zolper J C, Hagerott Crawford M, Pearton S J, Abernathy C R, Vartuli C B, Yuan C and Stall R A 1996 *J. Electron. Mater.* **25** 839
- [215] Liu C, Mensching B, Zeitler M, Volz K and Rauschenbach B 1997 *Phys. Rev. B* **57** 308
- [216] Lin C F, Chi G C, Feng M S, Guo J D, Tsang J S and Hong J M 1996 *Appl. Phys. Lett.* **68** 3758
- [217] Lee C-H, Chi G C, Lin C F, Feng M S and Guo J D 1996 *Appl. Phys. Lett.* **68** 3440
- [218] Ponce F A, Bour D P, Götz W and Wright P L 1996 *Appl. Phys. Lett.* **68** 57
- [219] Tan H H, Williams J S, Zou J, Cockayne D J H, Pearton S J and Stall R A 1996 *Phys. Lett.* **69** 2364
- [220] Pankove J I and Hutchby J A 1976 *J. Appl. Phys.* **47** 5387
- [221] Ilegems M and Dingle R 1973 *J. Appl. Phys.* **44** 4134
- [222] Menniger J, Jahn U, Brandt O, Yang H and Ploog K 1996 *Appl. Phys. Lett.* **69** 836
- [223] Hoffman D M *et al* 1995 *Phys. Rev. B* **52** 16702  
Hoffman A 1997 *Solid-State Electron.* **41** 275
- [224] Pong B J, Pan C J, Teng Y C, Chi G C, Li W-H, Lee K C and Lee C-H 1998 *J. Appl. Phys.* **83** 5992
- [225] Zolper J C, Han J, Van Deusen S B, Biefeld R, Crawford M H, Jun J, Suski T, Baranowski J M and Pearton S J 1998 *Mater. Res. Soc. Symp. Proc.* **482** 618

- [226] Strite S, Pelzmann A, Suski T, Leszczynski M, Jun J, Rocket A, Kemp M and Ebeling K J 1997 *MRS Internet J. Nitride Semicond. Res.* **2**
- [227] Zolper J C, Tan H H, Williams J S, Zou J, Cockayne D J H, Pearton S J, Crawford H M and Karlicek R F 1997 *J. Appl. Phys.* **70** 2927
- [228] Cao X A *et al* 1998 *Appl. Phys. Lett.* **73** 229
- [229] Sheu J K, Tsai M S, Wu W L, Kuo C H and Chi G C 2002 *J. Appl. Phys.* at press
- [230] Sheu J K, Chi G C and Jou M J 2001 *IEEE Electron. Devices Lett.* **22** 160–2
- [231] Kuo C H, Sheu J K, Chi G C, Huang Y L and Yeh T W 2001 *Solid-State Electron.* **45** 717–20
- [232] Sheu J K, Kuo C H, Chi G C, Chen C C and Jou M J 2002 *Solid-State Electron.* **45** at press
- [233] Tansly T L and Foley C P 1984 *Electron. Lett.* **20** 1066
- [234] Sheu J K, Su Y K, Chi G C, Pong B J, Chen C Y, Huang C N and Chen W C 1998 *J. Appl. Phys.* **84** 4590
- [235] Sheu J K, Tsai M S, Tun C J, Lee C C and Chi G C 2002 *J. Appl. Phys.* at press
- [236] Wen T C, Lee W I, Sheu J K and Chi G C 2001 *Solid-State Electron.* **45** 427–30